RSC Advances

REVIEW

View Article Online
View Journal | View Issue

Cite this: *RSC Adv.*, 2026, **16**, 17039

Biochar-supported photocatalysts for microplastics removal: mechanisms, material design, and pathways towards real-world applications

Ahmad K. Badawi, *[a] Raouf Hassan [b] and Bushra Ismail [c]

Microplastics (MPs) persist in ecosystems, are dispersed over long distances, and readily adsorb hazardous contaminants, posing a critical global threat. Biochar-supported photocatalysts (BSPs) have emerged as next-generation materials that influence the synergistic integration of biochar's physicochemical properties with the oxidative capabilities of semiconductor-based photocatalysis, enhancing the charge-transfer between the components and outperforming their conventional counterparts. In contrast to the previously published reviews, this review provides a comprehensive, mechanism-driven analysis of the degradation performance of MPs using BSP systems, connecting material architecture by integrating data from several disciplines, charge transfer dynamics, and reactive oxygen species (ROS) generation. Biochar's basic high surface area (up to 800 m^2 g^{-1}) and rich oxygen/nitrogen containing functional groups enable efficient adsorption of MPs onto the catalyst surface, significantly increasing light-driven reaction efficiency. Rather than discussing the performance of BSP systems in isolation, we adopted a mechanism driven integrated approach towards bridging the critical gap caused by the absence of any comprehensive framework. We summarized experimental findings indicating that BSPs can achieve significant removal of MPs under laboratory-specific conditions, with performance strongly dependent on composite architecture and reactor configuration. Various systems including ZnO/biochar, TiO_2/GO/biochar, and multi-heterojunction TiO_2/Fe_3O_4/graphene/biochar composites have demonstrated effective photocatalytic degradation of MPs. These outcomes should be interpreted as indicative of the potential of BSP systems rather than directly comparable performance metrics, since variations in light source, irradiation time, MP polymer type, particle size, catalyst loading, and reactor design can substantially influence the observed removal efficiency. We also highlighted novel design strategies including the fabrication of S-scheme and Z-scheme heterojunctions (*e.g.*, g-C_3N_4/$BiVO_4$/biochar and TiO_2/Fe_3O_4/biochar) that enhance electron hole separation rates by factors exceeding 5× relative to conventional photocatalysts. BSPs mitigate plastic pollution and achieve carbon-negative profiles *via* residue valorization. Advanced reactor types such as fluidized, fixed, and membrane-integrated ones show prospects for maximum performance w.r.t. MP removal, despite worries about stability, regeneration, and byproducts.

Received 19th January 2026
Accepted 20th March 2026

DOI: 10.1039/d6ra00463f

rsc.li/rsc-advances

1 Introduction

The ubiquity of microplastics (MPs) in global and aquatic ecosystems has intensified into one of the most urgent environmental challenges of the Anthropocene.[1,2] Recent studies estimate the presence of 51 trillion particles in global aquatic systems; updated monitoring continues to find MPs in remote marine and freshwater systems and in human consumables (seafood, drinking water, *etc.*).[2,3] A recent mesocosm study shows limited immediate trophic collapse but measurable sub-lethal physiological impacts[4,5] and another study shows inhalation/ingestion exposure routes in humans.[2,6]

MPs, defined as synthetic polymer fragments smaller than 5 mm, originate from primary sources such as microbeads in personal care products, industrial abrasives, and resin pellets, as well as secondary sources resulting from the fragmentation of larger plastic fragments through photochemical oxidation, mechanical abrasion, and biological degradation.[6,7] Their

[a]*Civil Engineering Department, El-Madina Higher Institute for Engineering and Technology, Giza 12588, Egypt. E-mail: dr.ahmedkaram91@gmail.com; Tel: +02-01114743578*

[b]*Civil Engineering Department, College of Engineering, Imam Mohammad Ibn Saud Islamic University (IMSIU), 11432 Riyadh, Saudi Arabia. E-mail: rahassan@imamu.edu.sa*

[c]*Department of Chemistry, COMSATS University Islamabad, Abbottabad Campus-22060, Pakistan. E-mail: bushraismail@cuiatd.edu.pk*

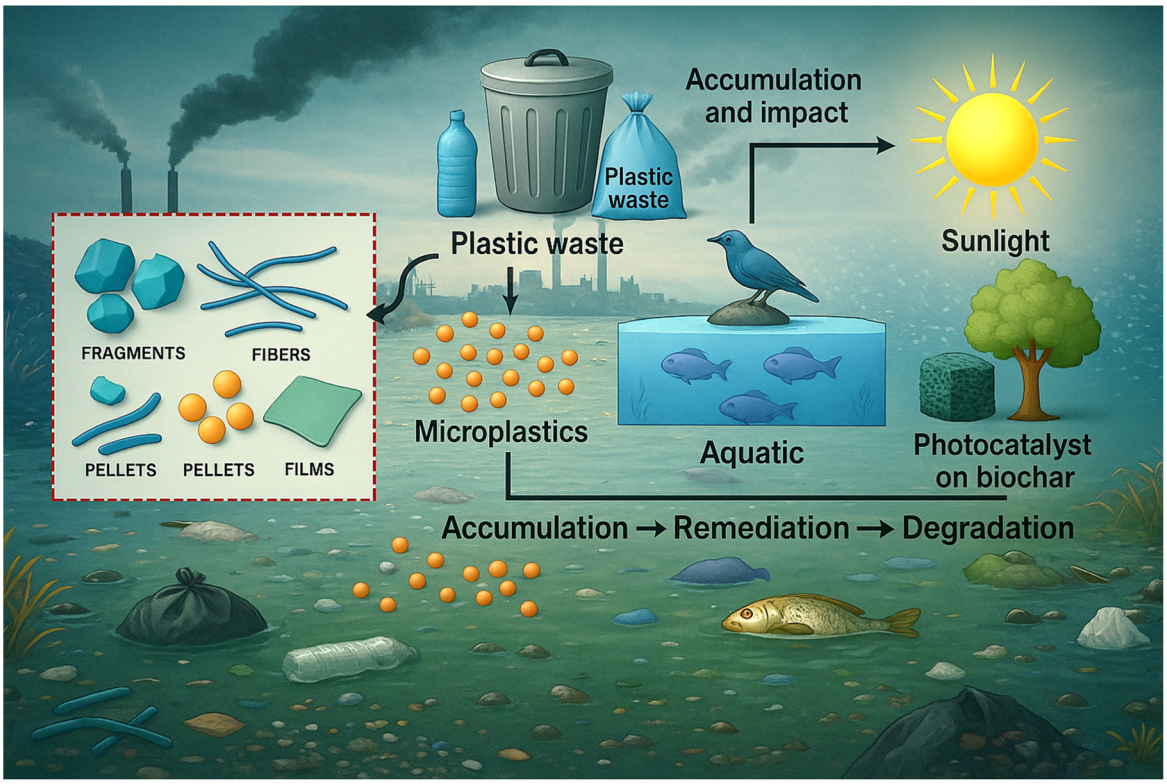

Fig. 1 Microplastic remediation schematic and microplastic classification by morphology.

persistence is a direct consequence of their intrinsic chemical stability, hydrophobicity, and high molecular weight, enabling them to resist microbial or enzymatic breakdown for decades.[8–10] This environmental persistence facilitates their accumulation across trophic levels, from plankton and benthic invertebrates to fish, seabirds, marine mammals, and ultimately human populations *via* dietary intake.[11,12] Fig. 1 presents a schematic overview of microplastic remediation pathways alongside a classification of MPs by morphology. Conventional wastewater treatment plants can capture a significant fraction of MPs, with advanced systems achieving removal efficiencies of up to 99%.[13–15] However, they continue to be insufficient barriers, discharging billions of particles annually into receiving waters.[3] Fibers smaller than 100 μm are particularly challenging, with capture efficiencies often falling below 50% due to their flexible morphology and low settling velocities.[2,3,16] The environmental risks of MPs extend beyond their physical presence, as their high surface area to volume ratio and hydrophobic surfaces enable them to adsorb and transport a wide spectrum of co-contaminants, including heavy metals, persistent organic pollutants, antibiotics, and pathogenic microorganisms.[17,18]

These interactions create complex mixtures with enhanced bioavailability and toxicity.[19,20] Laboratory studies have demonstrated that MPs can induce oxidative stress, neurotoxicity, endocrine disruption, and reproductive impairments in aquatic organisms.[17,21] While the human health impacts are less well characterized, emerging evidence suggests potential risks such as chronic inflammation, oxidative damage, and genotoxicity following ingestion or inhalation.[2,3] The complexity of MP pollution has prompted the exploration of advanced water treatment strategies capable of achieving complete removal and mineralization of MPs.[3] Among these, advanced oxidation processes (AOPs) have emerged as highly promising due to their ability to generate ROS that can oxidatively cleave polymer chains into smaller, environmentally benign molecules such as CO_2 and H_2O.[3,22] Biochar can activate persulfate/peroxymonosulfate/peroxide *via* surface-bound redox centers or transition metals (Fe), producing $SO_4^{\cdot-}$ and $^{\cdot}OH$; this complements photocatalytic ROS and can be combined in photo-Fenton or photo-persulfate hybrids to enhance degradation rates.[23,24] Semiconductor-based photocatalysis is particularly attractive because it can harness solar irradiation to drive these oxidation reactions, offering a low energy, sustainable approach.[25,26] Nevertheless, conventional photocatalysts face three critical limitations: the ultrafast recombination of photogenerated electron hole pairs, the restricted spectral response of many metal oxides to ultraviolet light, and the difficulty of separating and recovering nanoscale catalysts from treated water without secondary contamination.[21,27,28]

Biochar-supported photocatalysts (BSPs) present a transformative solution to these challenges by integrating the multifunctional properties of biochar with the oxidative capabilities of photocatalysis.[19,27] Biochar, derived from the thermochemical conversion of biomass such as agricultural residues, forestry waste, or municipal green waste under oxygen-limited conditions at 300–900 °C, offers a unique set of physicochemical attributes.[17,26]

These include hierarchical porosity and high specific surface area (200–800 m^2 g^{-1}), abundant oxygen and nitrogen containing functional groups (such as –COOH, –OH, and C=O), graphitic domains that facilitate electron conduction, and intrinsic persistent free radicals capable of stabilizing ROS.[13,29] When combined with semiconductor photocatalysts such as TiO_2, g-C_3N_4, or $BiVO_4$, biochar serves as both an adsorption scaffold and an electron mediator, enhancing mass transfer, suppressing charge recombination, extending light absorption into the visible spectrum, and enabling advanced heterojunction designs such as S-scheme and Z-scheme configurations.[21,27,28,30]

The environmental synergies of BSPs extend beyond performance metrics. The valorization of biomass waste into biochar not only diverts organic residues from open burning or landfill disposal but can also achieve net carbon negativity, with life cycle analyses reporting reductions of up to 2.3 kg CO_2 equivalent per kilogram of biochar produced.[31,32] This dual benefit of mitigating both carbon emissions and plastic pollution significantly strengthen the sustainability case for BSP adoption.[32] Recent technological developments have further improved BSP applicability, including the synthesis of magnetically recoverable composites for facile separation, the use of atomic layer deposition to enhance photocatalyst stability and interfacial bonding, and the application of machine learning algorithms to optimize biochar feedstock selection, pyrolysis conditions, and photocatalyst loading.[33,34] Despite these advances, several critical challenges remain. Long-term stability and reusability of BSPs in complex natural water matrices are yet to be fully demonstrated.[2,3] Comparing the performance of different BSPs is integrally challenging due to variations in experimental conditions across studies. Factors such as microplastic type (*e.g.*, PS, PE, PP), particle size, catalyst loading, light source and intensity, reaction time, and reactor configuration can significantly influence the observed degradation efficiencies. These variations often limit the direct comparability of reported removal percentages, highlighting the need for standardized experimental protocols. Therefore, normalized performance metrics such as quantum efficiency or apparent reaction rate constants are crucial for meaningful inter-system comparison. Standardized reporting will enable the evaluation of both lab-scale performance and practical applicability of different BSPs in microplastic degradation.[2,3]

The ecotoxicological implications of nanoplastics and intermediate degradation products require systematic investigation. Additionally, the design of scalable, cost-effective photoreactor systems remains a barrier to industrial implementation. Addressing these challenges will require interdisciplinary approaches that integrate materials science, environmental engineering, process intensification, and systems-level life cycle analysis.[3] Although several recent review articles have summarized photocatalytic materials for pollutant degradation, most of them primarily focus on material synthesis or general photocatalytic performance. In contrast, the present review adopts a mechanism-driven integrated perspective that explicitly connects material architecture, interfacial charge transfer pathways, reactive oxygen species (ROS) generation, and the resulting degradation behavior of microplastics. By organizing the discussion around these mechanistic links, the review aims to provide a deeper understanding of how structural design strategies translate into photocatalytic efficiency. Furthermore, the work integrates emerging heterojunction concepts such as S-scheme and Z-scheme systems, quantitative comparisons of degradation efficiencies, and sustainability considerations including carbon-negative biochar systems and reactor design. This integrated framework is intended to complement existing reviews by highlighting the mechanistic relationships that govern photocatalytic MPs degradation rather than merely summarizing material developments.

This review aims to (1) critically analyze state of the art BSP designs with emphasis on novel heterojunction architectures and functionalization strategies for enhanced MP removal; (2) clarify synergistic mechanisms between biochar and photocatalysts from molecular to macroscopic scales, focusing on charge transfer dynamics and ROS generation; (3) identify key scaling challenges and propose engineering solutions for field deployment; and (4) outline future research priorities to accelerate the transition of BSPs from laboratory prototypes to practical, sustainable MP remediation technologies.

2 Methodology

To conduct a critical review on biochar-supported photocatalysts (BSPs) for microplastics (MPs) removal, a systematic literature search was performed using two primary academic databases: Web of Science (WoS) and Scopus. These databases were selected for their extensive coverage of peer-reviewed scientific journals, conference proceedings, and book chapters spanning environmental science, materials science, chemical engineering, and related fields. The search encompassed publications from inception to August 2025, ensuring that the most recent advances in BSP technologies and their applications in MPs remediation were captured. The search strategy employed keywords and terms designed to cover the intersection of key thematic areas including biochar materials, photocatalysis, microplastics, and environmental remediation. Boolean operators AND and OR were used to combine these keywords systematically. The primary keywords and their variants included terms such as biochar; photocatalyst or photocatalysis; microplastic, microplastics, plastic particles, or plastic debris; removal, degradation, elimination, or treatment; hybrid materials or composite materials; ROS; charge transfer; electron–hole separation; S-scheme or Z-scheme heterojunction; sustainability, carbon negative, or life cycle assessment (LCA); and green technology or environmental remediation.

An example of the combined search string used in Scopus and Web of Science was: ("biochar" AND ("photocatalyst" OR "photocatalysis") AND ("microplastic" OR "plastic debris") AND ("removal" OR "degradation" OR "treatment") AND ("hybrid" OR "composite") AND ("ROS" OR "reactive oxygen species") AND ("charge transfer" OR "electron–hole separation") AND ("S-scheme" OR "Z-scheme") AND ("sustainability" OR "life cycle

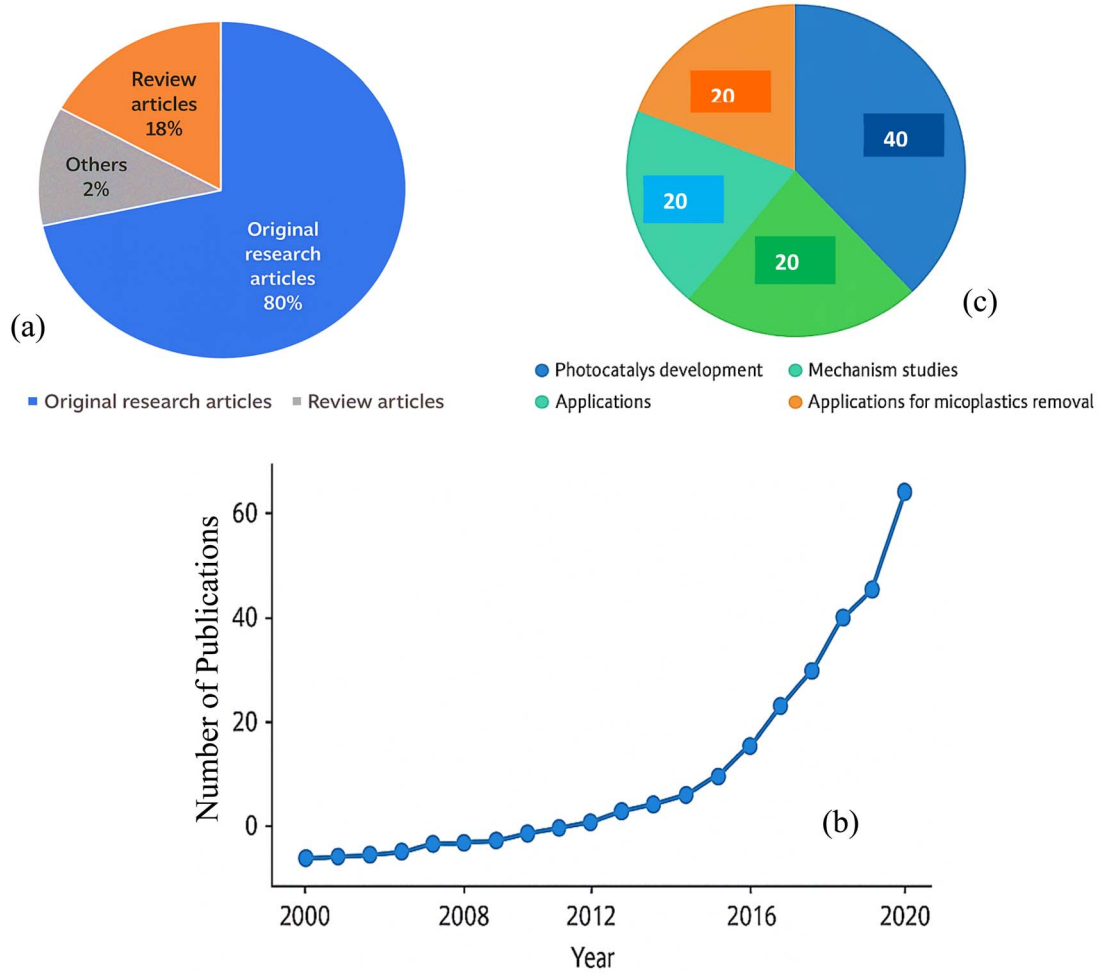

Fig. 2 (a) Distribution of reviewed publications by type, (b) the annual publication count and (c) the distribution of publications across biochar-supported photocatalysis research areas.

assessment" OR "carbon negative"). Inclusion criteria for selecting relevant publications comprised peer-reviewed articles, reviews, conference papers, and book chapters that focused on the synthesis, characterization, and application of biochar-supported photocatalysts specifically for MPs removal or degradation. Studies investigating mechanisms such as ROS generation, charge transfer, and heterojunction design in BSPs were also included, alongside publications reporting experimental results, pilot-scale studies, or theoretical insights related to the environmental sustainability and life cycle assessments of BSPs. Conversely, studies that exclusively focused on photocatalysts without biochar support, research limited to bulk plastics rather than micro or nano plastics, articles not published in English, and non-peer-reviewed reports or gray literature were excluded to maintain relevance and quality. Following the initial search, duplicate records were removed, and titles and abstracts were screened to exclude irrelevant publications. The full texts of the remaining papers were then retrieved and critically assessed for relevance and methodological quality. Data extraction involved gathering publication metadata including year, journal, and publication type; details on the types of biochar and photocatalysts used; descriptions of photocatalytic mechanisms such as ROS types and charge carrier dynamics; types and concentration ranges of MPs treated; experimental conditions and performance metrics like removal efficiency and kinetics; sustainability assessments including carbon footprint and life cycle analysis; as well as discussions on challenges and future outlooks.

Finally, bibliometric data were tabulated and visualized to illustrate research trends, publication growth, and the distribution of research outputs by type and geographic origin. Fig. 2(a) presents the distribution of reviewed publications by type. Original research articles constitute the majority of the literature, followed by review articles, reflecting a robust foundation of empirical studies alongside a growing interest in synthesizing existing knowledge. The Fig. 2(b) also illustrates the annual publication trends, revealing the temporal evolution of research in this field. A pronounced upward trajectory is evident in recent years, underscoring the increasing scholarly attention and research efforts dedicated to biochar-supported photocatalysts for microplastics removal. Additionally, Fig. 2(c) highlights the distribution of publications across key research domains within this field, providing insight into dominant themes and emerging areas of interest.

3 Biochar as a sustainable platform for photocatalytic systems

The efficacy of BSPs hinges on the physicochemical properties of biochar, which are naturally linked to biomass feedstock selection and pyrolysis conditions.[17,26] Recent advances have demonstrated that lignocellulosic feedstocks (*e.g.*, pine, bamboo, and rice husk) yield biochar with superior photocatalytic support capabilities compared to sludge derived alternatives, owing to their higher carbon content (65–85 wt%) and more developed porous architectures.[13,35,36] Fig. 3 presents the comparison of biochar feedstocks and their properties for photocatalyst support. Pyrolysis temperature develops as the most critical parameter, inducing distinct structural transformations across three key stages: hemicellulose decomposition (300–400 °C) creating micropores, cellulose degradation (400–600 °C) developing mesopores, and lignin breakdown (>600 °C) initiating graphitization.[13,26,35] Systematic studies expose that the optimal temperature window for photocatalytic supports lies between 500–650 °C, balancing porosity development with retention of oxygen functional groups essential for catalyst anchoring.[26] For instance, bamboo biochar pyrolyzed at 650 °C achieves a remarkable surface area of 720 $m^2\ g^{-1}$ with 3.2 nm average pore diameter, while maintaining 8.2 mmol g^{-1} of oxygen containing groups critical for hydrophilic MP adsorption.[13,26]

Post-synthesis modifications further enhance biochar's suitability as a photocatalytic support. These engineered properties collectively address the tripartite requirements for ideal photocatalytic supports: (1) high surface area (>300 $m^2\ g^{-1}$) for MP adsorption and catalyst dispersion, (2) electron-conducting networks (resistivity <10 Ω cm) to mitigate charge recombination, and (3) optimal surface chemistry (O/C ratio 0.2–0.4) for stable catalyst anchoring. The environmental sustainability of biochar production adds another dimension to its appeal.[17,31] Life-cycle assessments demonstrate that converting agricultural residues to biochar reduces net greenhouse gas emissions by 2.3 kg CO_2 equivalent per kg biochar produced, while simultaneously addressing waste management challenges.[37] For example, utilizing rice husk a globally rich agro-waste typically burned in open fields as biochar feedstock prevents 1.8 kg CO_2 per kg emissions from uncontrolled combustion.[15,19]

When paired with photocatalytic functionality, these systems achieve dual environmental benefits: (1) valorization of waste biomass into high-value materials and (2) solar-driven remediation of microplastic pollution.[38,39] Synchrotron-based X-ray absorption spectroscopy (XAS) has identified charge transfer pathways at Ti–O–C bonds in TiO_2-biochar systems, while *in situ* electron paramagnetic resonance (EPR) quantifies the critical role of persistent free radicals (0.5–2.0 spins per mg) in prolonging ROS lifetimes.[2,19,40] Machine learning algorithms successfully correlate biochar properties (pyrolysis temperature, O/C ratio, pore size distribution) with photocatalytic efficiency ($R^2 = 0.91$ for MP degradation rate predictions).[17,22,41]

4 Biochar-photocatalyst integration methods

The method of integrating biochar with photocatalysts plays a key role in determining the composite's morphology, surface

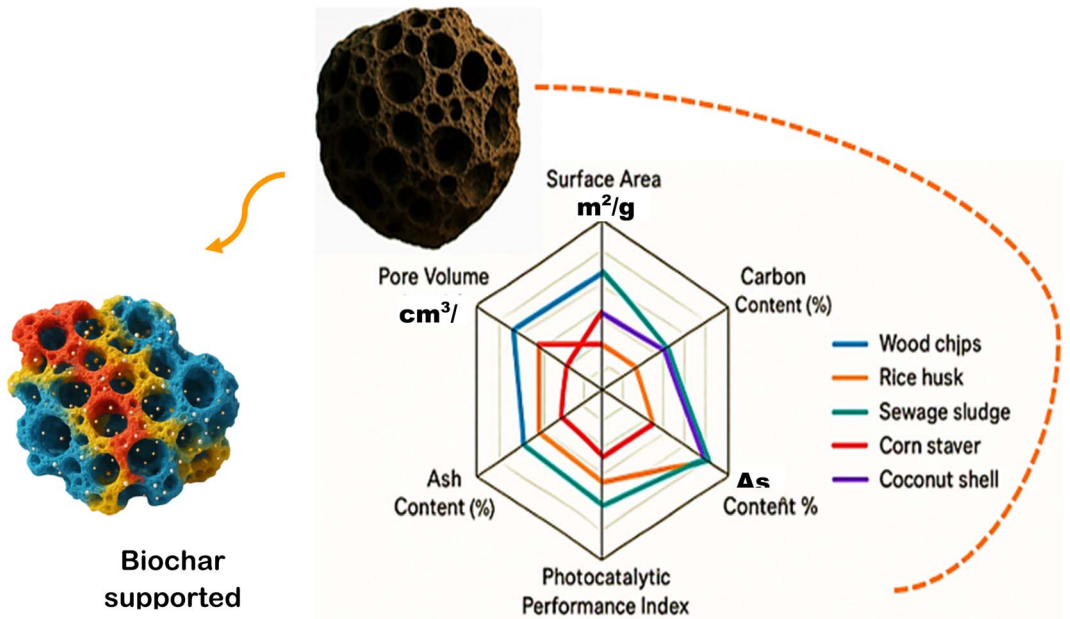

Fig. 3 Comparison of biochar feedstocks and their properties for photocatalyst support.

chemistry, interfacial contact, and ultimately its photocatalytic efficiency.[17,18] A wide range of synthesis approaches has been explored, each offering distinct advantages and limitations that directly influence the electron transfer pathways, active site exposure, and stability of the resulting materials.[25,31] For instance, TiO_2-biochar composites prepared through sol–gel synthesis have achieved up to 93% degradation of dimethyl phthalate (DMP), highlighting their potential for organic pollutant treatment.[1,42] However, optimization of pore structure remains necessary to maximize efficiency in microplastics and emerging contaminant removal.[7,41]

The hydrothermal and solvothermal methods offer superior control over crystal structure and particle size while simultaneously promoting strong interfacial bonding between the photocatalyst and biochar surface.[22,43] This process typically operates under high pressure and temperature conditions, enabling the formation of well-crystallized nanoparticles intimately anchored onto biochar's functionalized surface.[44,45] Although energy intensive, this method yields composites with enhanced stability and electron transport efficiency.[43,44] For example, ZnO/biochar composites synthesized hydrothermally demonstrated an impressive 99.67% dye degradation, attributed to the creation of abundant heterojunction interfaces that facilitate rapid electron–hole separation.[43,44] The strength of hydrothermal composites makes them highly promising for long-term photocatalytic operations in aquatic environments.[44,46] The ultrasound-assisted method has emerged as an energy-efficient alternative, relying on cavitation-induced shock waves to promote intimate mixing and uniform deposition of nanoparticles on biochar.[47,48]

Operating at relatively low temperatures, this technique enables the formation of highly dispersed photocatalyst layers without excessive agglomeration.[47] TiO_2 immobilized on wood-pellet-derived biochar *via* ultrasound-assisted synthesis showed improved dispersion and enhanced photocatalytic activity, suggesting its suitability for low-energy, environmentally friendly synthesis routes.[49,50] However, scaling up ultrasound-based processes remains challenging due to difficulties in maintaining consistent cavitation effects across larger reaction volumes.[49,50] The *in situ* growth method represents one of the most effective strategies for fabricating BSP with intimate interfacial contact.[51,52] In this process, photocatalyst precursors are directly nucleated and grown on biochar substrates, minimizing aggregation and maximizing charge transfer efficiency.[52] The resulting composites often show chemical bonding between the photocatalyst and biochar functional groups, significantly improving durability and electron mobility.[51,52] A notable example includes g-C_3N_4 nanosheets directly grown on biochar fibers, which demonstrated superior photocatalytic degradation performance due to the formation of highly efficient heterojunctions.[53] Despite its promise, *in situ* growth can be complex and time-consuming, often requiring exact control of reaction conditions.[54]

On the other hand, mechanical mixing offers a straightforward and highly scalable route to composite preparation.[26,55] In this approach, biochar and photocatalyst powders are physically mixed using grinding or milling, producing composites with minimal chemical modification.[55] While attractive for large-scale applications due to its simplicity and low cost, this method often results in weak interfacial bonding and poor charge transfer properties. For instance, Sb_2O_3–$Ce_2Sn_2O_7$ supported on coffee husk biochar synthesized by simple mixing demonstrated functional adsorption and degradation properties, but its overall photocatalytic efficiency was limited compared to chemically bonded systems.[56,57] Comprehensive characterization is essential for correlating the BSPs with their photocatalytic performance in MPs degradation. X-ray diffraction (XRD) determines crystalline phases and confirms the formation of heterojunctions (*e.g.*, anatase/rutile TiO_2 or $BiVO_4$–g-C_3N_4 interfaces), while identifying the degree of graphitization of the biochar matrix. The characteristic diffraction peak at $2\theta = 25°$ corresponds to the (002) plane of graphitic carbon, and additional reflections indicate metal oxide incorporation or phase transitions during thermal synthesis.[58]

Field-emission scanning electron microscopy (FESEM) and transmission electron microscopy (TEM) elucidate the dispersion of nanoparticles on the biochar surface and the nanoarchitecture of heterojunctions. TEM (HRTEM) images confirm lattice fringes (*e.g.*, 0.35 nm for anatase TiO_2 (101) and intimate contact between crystalline domains and graphitic carbon layers, which enables efficient interfacial electron transfer. Brunauer–Emmett–Teller (BET) analysis quantifies surface area and porosity. Fourier-transform infrared spectroscopy (FTIR) identifies functional groups (–OH, –COOH, C=O, and C–O–C) responsible for adsorption of microplastics and anchoring of metal oxides. Shifts or disappearance of peaks after catalyst modification confirm chemical interactions and surface oxidation. Advanced techniques such as high-resolution TEM, X-ray photoelectron spectroscopy (XPS), and time-resolved photoluminescence (TRPL) have revealed that hydrothermal and *in situ* growth methods generally establish stronger chemical bonds and better interfacial architectures compared to physical mixing techniques.[26,55,57]

A key method for understanding the electrical structure and surface chemistry of biochar-supported photocatalysts is X-ray photoelectron spectroscopy (XPS) as shown in Fig. 4. This technique helps identify oxidation states and elemental composition, confirming the presence of dopants and functional groups that influence photocatalytic activity. For instance, changes in binding energy for Ti 2p or Cu 2p peaks can indicate the formation of heterojunctions, while an increase in reactive oxygen species (ROS) production is linked to oxygen vacancies observed in O 1s spectra. To design effective photocatalysts for environmental applications-like removing microplastics, degrading dyes, and breaking down antibiotics-these insights are vital.

When it comes to understanding how charge carriers behave in photocatalysts, Time-Resolved Photoluminescence (TRPL) is a central technique. The decay profiles from TRPL reveal that biochar-based composites have longer lifetimes compared to pure semiconductors, which suggests that they achieve better charge separation and reduced recombination as shown in Fig. 5. This improvement is largely due to the conductive network and the formation of heterojunctions in biochar, which

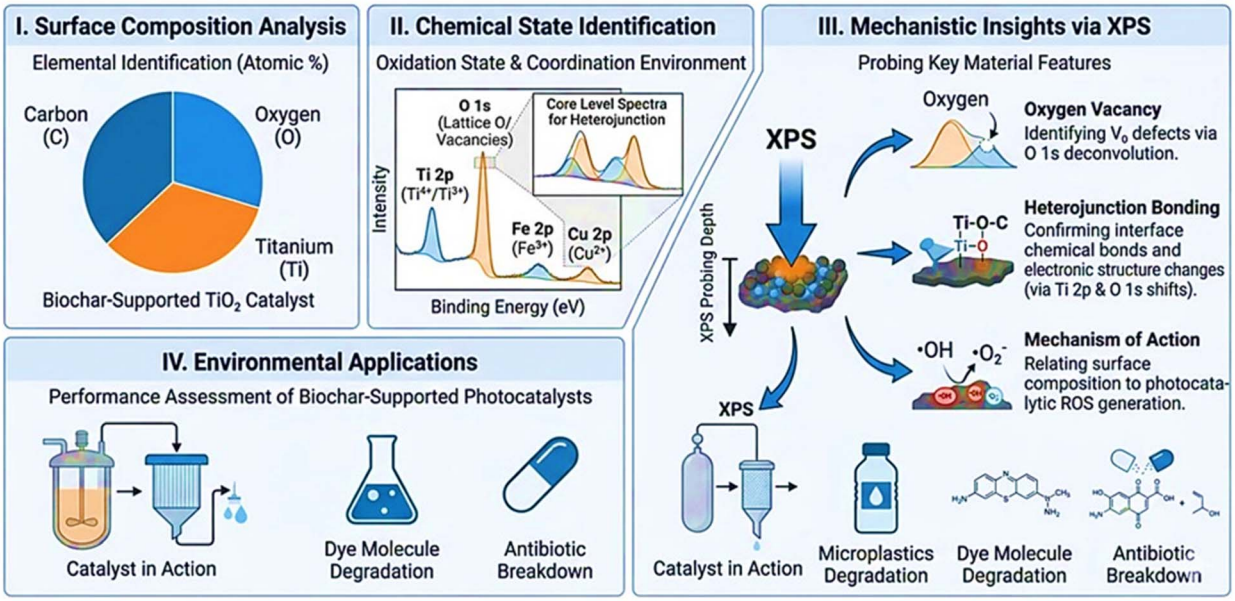

Fig. 4 Diagrammatic illustration of XPS role in determination of surface composition including elements like carbon (C), oxygen (O), and any dopants, chemical states of these elements, such as Cu^{2+} and Fe^{3+}, along with important mechanistic features like oxygen vacancies and heterojunction bonding.

facilitate electron movement and help stabilize the charges generated by light. The extended lifetimes also play a significant role in speeding up the breakdown of MPs and other pollutants, as they are directly linked to increased production of ROS. For example, g-C_3N_4/biochar systems show even greater advantages thanks to the π–π interactions between biochar and polymeric photocatalysts, while TiO_2/biochar composites can have lifetimes that are up to five times longer than those of pure TiO_2. These findings underscore the importance of TRPL in guiding the development of materials for high-performance photocatalytic applications.

These stronger biochar–photocatalyst interactions translate into enhanced charge separation, suppressed electron–hole recombination, and improved long-term stability. Thus, while simple methods like mechanical mixing may be useful for proof of concept or low-cost applications, hydrothermal and *in situ* approaches are more favorable for developing high performance composites aimed at MPs degradation and other advanced water treatment applications.

5 Photocatalyst design and heterojunction engineering

The photocatalytic performance of biochar-supported systems is fundamentally governed by the selection and engineering of

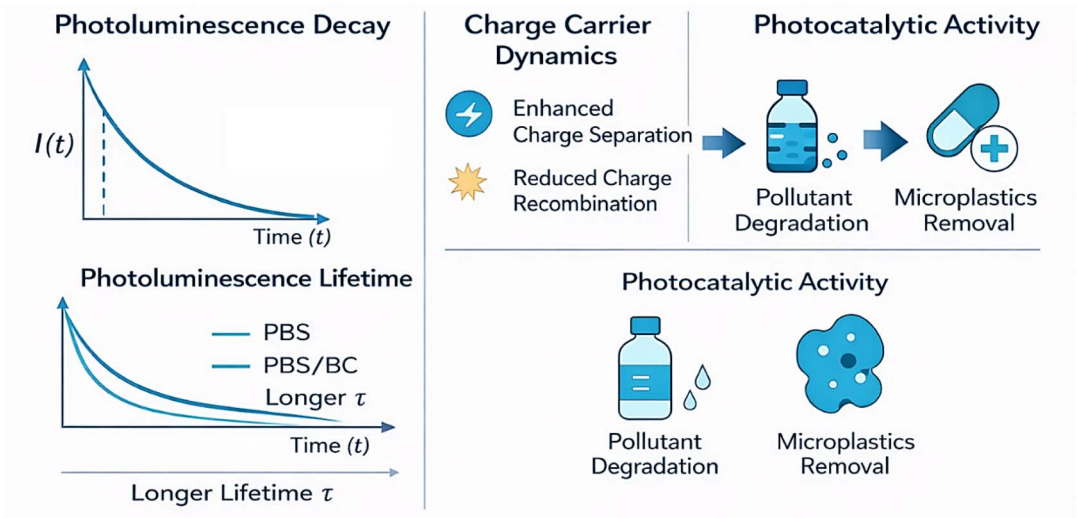

Fig. 5 Diagrammatic representation of TRPL analysis for photocatalysts supported by biochar. TRPL reveals charge carrier dynamics by measuring photoluminescence decay durations (τ).

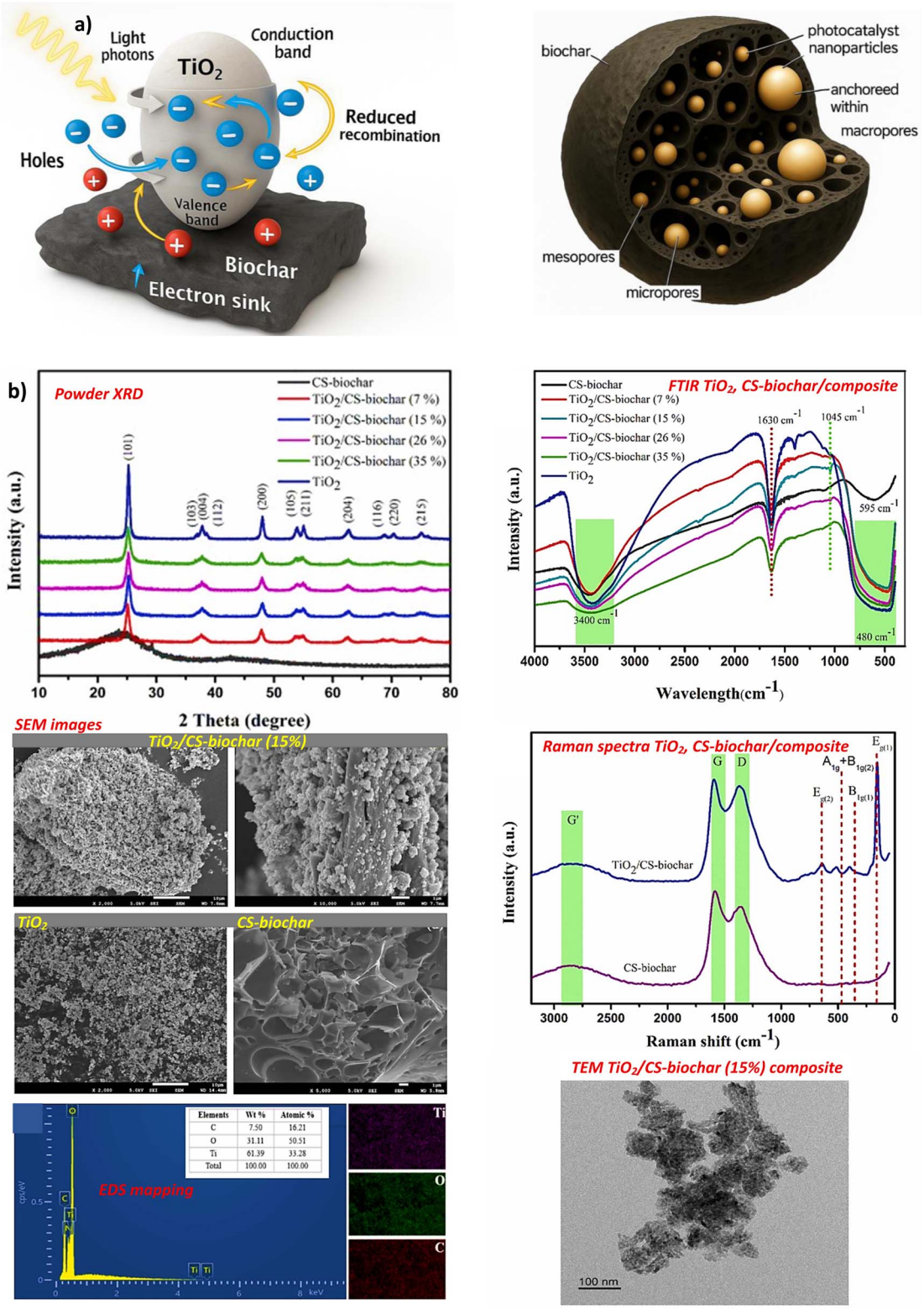

Fig. 6 (a) Enhanced photocatalytic activity mechanism of biochar-supported photocatalysts and (b) structural and surface characterization of TiO_2, CS-biochar and TiO_2/CS-biochar composites confirming the composite formation and interfacial bonding, adapted with permission from ref. 63, Copyright, Elsevier, 2022.

semiconductor components, which must satisfy stringent criteria including visible light responsiveness, suitable band edge positions, and stability in aqueous environments.[26,55] Recent studies have established that conventional wide-bandgap photocatalysts like TiO_2 (3.2 eV) and ZnO (3.3 eV) require structural modifications to achieve practical MP

degradation efficiencies under solar irradiation. Bandgap engineering through nitrogen doping reduces TiO_2's activation energy to 2.8 eV, extending light absorption to 450 nm while maintaining the strong oxidative potential (+2.9 V *vs.* NHE) needed for polymer chain scission.[59,60] Similarly, sulfur-doped g-C_3N_4 demonstrates a narrowed bandgap (2.4 eV *vs.* pristine 2.7 eV) and 3.2× higher $^{\cdot}OH$ generation rates for polyethylene degradation, attributed to enhanced charge separation and mid-gap states introduced by dopant atoms.[61,62]

Fig. 6(a) illustrates the structural composition and photocatalytic mechanism of a biochar-supported photocatalyst system. The left panel details the porous structure of biochar, highlighting macropores, mesopores, and micropores, within which photocatalyst nanoparticles (*e.g.*, TiO_2) are anchored. The right panel depicts the enhanced photocatalytic process: upon irradiation with light photons, electrons are excited from the valence band to the conduction band of the TiO_2 photocatalyst, generating electron–hole pairs. The biochar acts as an efficient electron sink, facilitating the transfer of electrons from the TiO_2 conduction band to the biochar surface, thereby significantly reducing electron–hole recombination and enhancing the overall photocatalytic efficiency.[17,41,42] Fig. 6(b) shows a full structural and surface characterization of a solid-phase fabrication of TiO_2/Chitosan-biochar composites with driven photocatalytic degradation performance.

The Raman spectra as shown in Fig. 6(b) provide crucial insights into how TiO_2 interacts with biochar in the composite. We can see that the crystalline structure of TiO_2 remains intact after forming the composite, as evidenced by the unique bands at approximately 144, 395, 514, and 638 cm^{-1}, which align with the E_g, $B1_g$, $A1_g$, and E_g vibrational modes of the anatase phase. In contrast, the prominent D (1350 cm^{-1}) and G (1590 cm^{-1}) bands of biochar reveal the presence of graphitic and disordered carbon structures. The slight shifts and changes in intensity of these peaks in the CS-biochar/TiO_2 composite suggest strong interfacial contacts and some electron transfer between the carbon framework and TiO_2, which can enhance charge separation during photocatalysis.

Additionally, the EDS elemental mapping as shown in Fig. 6(b) confirms a consistent spatial distribution of Ti, O, and C throughout the composite, demonstrating that TiO_2 nanoparticles have been effectively integrated into the biochar surface. This uniform distribution promotes the formation of a close heterojunction, ultimately boosting both the stability and efficiency of photocatalytic processes.

Despite the significant improvements in photocatalytic activity reported for S-scheme and Z-scheme heterojunction systems, several practical limitations remain. Many studies demonstrate enhanced performance under controlled laboratory irradiation conditions, which may not accurately represent real environmental scenarios. In addition, the stability of interfacial charge transfer pathways under long-term operation is still insufficiently investigated. Photocorrosion, catalyst surface fouling, and structural degradation can gradually reduce efficiency during repeated use. Therefore, future studies should focus not only on constructing advanced heterojunction architectures but also on evaluating their long-term stability, regeneration capability, and resistance to environmental interference such as dissolved organic matter and inorganic ions.

Heterojunction design has emerged as one of the most effective strategies to overcome intrinsic limitations of single-component photocatalysts, particularly their restricted light absorption ranges and high charge recombination rates. Biochar not only provides a strong structural platform but also serves as an efficient electron mediator its graphitic domains, high surface area, and surface functionalities enable heterojunction architectures difficult to achieve with conventional supports. This multifunctionality allows biochar-based heterojunctions to simultaneously enhance light harvesting, promote charge separation, and improve stability during prolonged operation. Recent developments in photocatalytic nanocomposites have demonstrated that both S-scheme and Z-scheme heterojunction architectures markedly improve redox efficiency by enhancing charge separation and preserving high oxidation-reduction potentials. In Z-scheme heterojunctions, photogenerated electrons in the conduction band (CB) of one semiconductor recombine with holes in the valence band (VB) of the other semiconductor, while the remaining high-energy electrons and holes remain spatially separated to participate in redox reactions.

The combination of biochar acts as a conductive π-conjugated mediator that accelerates interfacial electron transfer, maintains Fermi-level equilibrium, and anchors MPs near reactive sites, thus enhancing the localized generation of ROS such as $^{\cdot}OH$ and $^{\cdot}O_2^-$.[64,65] Conversely, the S-scheme heterojunction employs built-in internal electric fields and band bending to promote selective recombination of low-energy carriers while retaining high-energy electrons and holes on opposite semiconductor components.[66] This structure effectively suppresses charge recombination, as confirmed by TRPL and electrochemical impedance spectroscopy (EIS), which demonstrate increased carrier lifetimes and decreased charge transfer resistance.[67,68] Biochar in such systems acts as both an electron sink and defect-passivation network, stabilizing heterointerfaces and facilitating efficient electron migration.[69]

The mechanistic distinction between these two systems is critical for optimizing BSP performance in MP degradation. Z-schemes tend to favor strong reduction and oxidation sites, making them suitable for polymeric substrates requiring both oxidative cleavage and partial reduction steps, whereas S-schemes exhibit superior ROS sustainability under visible light due to their enhanced charge retention and interfacial field-driven selectivity.

To attack the issue of microplastics, let's take a look at the comparison schematic that illustrates the Z-scheme and S-scheme charge transfer mechanisms in biochar-supported photocatalysts as shown in Fig. 7. The Z-scheme system is quite clever; it keeps high oxidative and reductive potentials at opposite ends by allowing electrons from one semiconductor's conduction band to recombine with holes in another's valence band. This setup encourages the formation of ROS, which specifically target polymer chains and speed up the breakdown of microplastics.

On the flip side, the S-scheme mechanism employs band bending and an internal electric field to selectively recombine

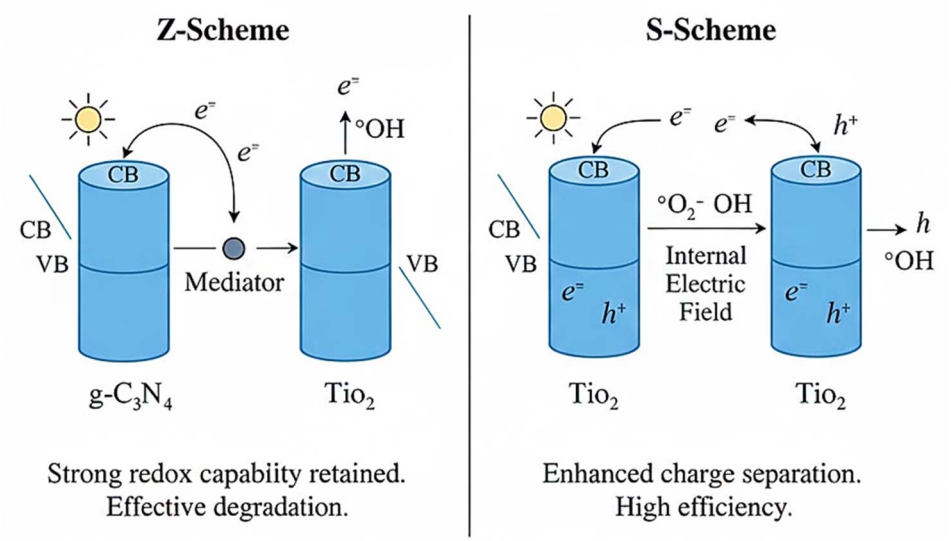

Feature	Z-Scheme	S-Scheme
Driving Force	Electron mediator or direct contact	Higher
Charge Separation	Modrate	Excellent
Degradation Efficiency	Good	Superior

Fig. 7 Comparative schematic of Z-scheme and S-scheme charge transfer mechanisms in biochar-supported photocatalysts for microplastics removal.

low-energy carriers, which leaves high-energy electrons and holes available for photocatalytic processes. This approach shines in practical applications because it achieves excellent charge separation and stability without needing external mediators. While both methods enhance photocatalytic performance, S-scheme systems often provide better long-term efficiency due to their inherent electrostatic driving force.

Together, these architectures demonstrate the critical role of heterojunction band engineering and biochar interfacial conductivity in next-generation photocatalytic systems for water purification and MPs remediation. Defect engineering and morphology control have recently emerged as key design principles for optimizing the catalytic and electronic behavior of BSPs in environmental remediation. The deliberate introduction of oxygen vacancies, heteroatom dopants (*e.g.*, N, S, Fe, B), and carbon lattice disorders significantly modifies the electronic density of states of both the semiconductor and biochar phases. These modifications create mid-gap states and shallow donor levels that narrow the bandgap, enhance visible-light absorption, and facilitate interfacial charge transfer.[70,71]

Oxygen vacancies in particular act as electron-trapping sites, prolonging charge-carrier lifetimes and accelerating the activation of dissolved oxygen into ($^{\bullet}O_2^-$), which subsequently form ($^{\bullet}OH$) *via* secondary reactions.[71,72] In parallel, heteroatom doping introduces surface polarity and additional defect orbitals (*e.g.*, N 2p or S 3p), which strengthen biochar semiconductor bonding and improve Fermi-level alignment, leading to enhanced electron–hole separation and faster redox kinetics.[71,73] Moreover, morphology control plays a vital role in dictating photon utilization, charge migration, and pollutant accessibility. Tailoring particle size, pore hierarchy, and surface roughness directly affects light scattering, adsorption, and catalytic site exposure. Biochar produced at moderate pyrolysis temperatures (500–700 °C) typically exhibits hierarchical micro-mesoporous structures and high specific surface areas exceeding 600 $m^2\ g^{-1}$, which enhance both the physical adsorption of MPs and the photon–matter interaction efficiency.[74]

Furthermore, biochar composites synthesized through *in situ* growth or hydrothermal anchoring promote intimate semiconductor biochar interfaces, which markedly reduce charge-transfer resistance and improve mechanical stability, as verified by EIS and high-resolution transmission electron microscopy (HRTEM) analyses.[71,72] The presence of ultrafine pores (<10 nm) additionally facilitates the confinement of reactive species and promotes short diffusion pathways for ROS generation near adsorbed MP surfaces.[74] Integrating defect-rich and morphologically optimized BSPs therefore provides dual

Table 1 Comparative analysis of heterojunction configurations on biochar supports

Heterojunction type	Example system	Charge separation efficiency (%)	MP degradation rate (h^{-1})	Key advantage	Ref.
Type-II	TiO_2/CuO/biochar	68	0.32	Spatial redox separation	78
S-scheme	g-C_3N_4/$BiVO_4$/biochar	92	0.85	Preserves strong redox potentials	75
Z-scheme	TiO_2/Ag/Ag_3PO_4/ biochar	78	0.45	Broad spectrum utilization	76 and 77
p–n Junction	Cu_2O/TiO_2/biochar	85	0.61	Built-in electric field	78

benefits enhanced light harvesting and accelerated redox kinetics resulting in efficient degradation of diverse MPs, including PE, PP, and PS. Such architectures also exhibit superior recyclability and stability, maintaining >85% of their photocatalytic activity after multiple degradation cycles due to robust interfacial binding and defect-regulated charge retention.[71,73]

Table 1 lists a comparative analysis of heterojunction configurations on biochar supports. A representative approach is the Z-type heterojunction photocatalyst composed of pre-graphitized g-C_3N_4 (PCN)/N-doped biochar/$BiVO_4$, in which N-biochar acts as a conductive channel to promote charge separation. This system achieved 92.5% degradation of norfloxacin under visible light and retained good stability over four cycles.[75] Although a direct S-scheme g-C_3N_4/$BiVO_4$/biochar system with PET degradation hasn't been reported yet, this work exemplifies how biochar facilitates charge transfer and heterojunction formation. Regarding Z-scheme designs, while the specific tri-component TiO_2/Ag/Ag_3PO_4 on magnetic biochar for PP degradation hasn't been documented in microplastics degradation literature, biochar-supported Ag_3PO_4 systems have demonstrated enhanced photocatalytic stability.

For example, Ag_3PO_4 nanoparticles supported on biochar ("AP/PBB") exhibited synergistic adsorption-photodegradation (*e.g.*, methylene blue removal) and improved charge management due to the biochar scaffold.[76,77] This reinforces the premise that biochar can suppress Ag_3PO_4 photocorrosion and serve as a stabilizing, electron-mediating support.

6 Mechanistic understandings into MPs degradation pathways

The degradation of MPs on BSPs occurs through a synergistic "adsorb and react" mechanism, where biochar acts as both an adsorptive concentrator and an electron mediator. The porous, π-conjugated structure of biochar (surface area often >500 m^2 g^{-1}) concentrates MPs and dissolved oxygen near photocatalytic sites *via* hydrophobic, π–π, and hydrogen-bond interactions.[79,80] Upon visible-light irradiation, photogenerated electrons (e^-) from the semiconductor migrate to the conductive biochar, while holes (h^+) remain in the valence band. This separation suppresses e^-/h^+ recombination and enhances the formation of ROS including hydroxyl ($^{\bullet}OH$), superoxide ($^{\bullet}O_2^-$), and singlet oxygen ($^1O_2$) that subsequently attack polymer chains at the adsorbed interface.[4,81] The interaction between adsorption and photocatalysis is highly polymer-specific.

For aliphatic polymers such as PE and PP, which contain easily abstractable C–H bonds, surface-bound $^{\bullet}OH$ radicals initiate hydrogen abstraction followed by oxygen insertion, leading to chain scission and oxidation into carboxylates and CO_2.[81,82] For aromatic polymers (*e.g.*, polystyrene, PS), π–π stacking with biochar graphitic domains enhances adsorption and ROS proximity, but the higher bond dissociation energy of aromatic C–C bonds necessitate prolonged irradiation or participation of more oxidizing species ($^{\bullet}O_2^-$, $^1O_2$). Oxygenated polymers such as PET or polyamide (PA) exhibit hydrogen bonding with –COOH/–OH groups on biochar, enabling hydrolysis and photo-Fenton-like attack at ester or amide linkages.

6.1 Adsorption and surface activation

The initial interaction between MPs and BSPs is primarily dictated by physicochemical adsorption, which plays a critical role in concentrating MPs at or near the catalytic active sites. This pre-concentration effect not only increases the probability of subsequent photocatalytic attack but also influences the selectivity and efficiency of degradation pathways.[4,81] *In situ* atomic force microscopy (AFM) and spectroscopic studies have consistently demonstrated that the adsorption step is highly polymer-specific and strongly dependent on the surface chemistry of biochar.[81] Three major mechanisms are generally identified as governing this adsorption process. First, hydrophobic interactions dominate when dealing with non-polar polymers such as PE and PP. These polymers exhibit limited solubility in aqueous environments, and their affinity for the hydrophobic, graphitic domains of biochar provides a favorable driving force for attachment, with reported binding energies of approximately 50 kJ mol^{-1}.[81,83]

Such interactions are particularly important in natural water systems, where hydrophobicity acts as a major determinant of MP mobility and partitioning.[81] Second, hydrogen bonding becomes critical when oxygen-containing functional groups are present in MPs such as PET or nylon.[82,84] The carboxyl and hydroxyl groups on the biochar surface can form directional hydrogen bonds with carbonyl or amide groups in these polymers, thereby enhancing adsorption affinity.[82] This interaction is further strengthened when biochar is chemically modified (*e.g.*, through oxidation or nitrogen doping), which increases the density of polar functional groups.[4,82] Third, π–π stacking interactions play a dominant role in the adsorption of aromatic polymers such as PS.[84] The conjugated aromatic rings of PS interact with the polyaromatic sheets within biochar's carbon

matrix, forming strong stacking interactions that effectively immobilize MPs on the catalyst surface.[82,84] This mechanism is mainly relevant because PS tends to resist degradation due to its aromatic backbone, and surface anchoring *via* π–π stacking significantly increases the efficiency of ROS attack by ensuring intimate polymer-catalyst contact.[81,82]

Beyond these three primary mechanisms, adsorption can also be modulated by electrostatic interactions, especially when MPs undergo environmental aging.[4,81] Oxidized MPs often attain negatively charged surfaces, which can interact with positively charged sites on biochar or with loaded metal/metal-oxide nanoparticles.[4,82] Conversely, alkaline or high ionic strength water conditions can suppress such electrostatic interactions, highlighting the importance of environmental context in determining adsorption efficiency.[4,82] Collectively, these mechanisms demonstrate that adsorption is not a passive step but an active determinant of photocatalytic efficiency.

Moreover, adsorption provides a crucial "surface activation" effect, whereby MPs are oriented and anchored in close proximity to photocatalytic centers, thereby reducing charge transfer distances and accelerating degradation kinetics. This dual role of adsorption as both a pre-concentration and activation step underpins the superior performance of BSPs in MPs remediation and highlights opportunities for rational design of surface engineered biochar photocatalyst composites.

6.2 ROS generation and polymer attack

In the adsorption and surface activation phase, the degradation of MPs on BSPs is driven by the generation of ROS under light irradiation. The mechanistic pathways for MPs degradation vary significantly with the heterojunction architecture of the BSP. Type-II, Z-scheme, and S-scheme heterojunctions exhibit distinct charge separation and electron transfer dynamics. Biochar plays multiple roles in these architectures, including enhancing electron transport, promoting interfacial charge separation, and facilitating the generation of ROS.[1,85] Variations in the catalyst architecture directly influence the dominant oxidative pathways, affecting both degradation efficiency and reaction selectivity. Such mechanistic distinctions must be considered when comparing the performance of different BSP systems. Upon photoexcitation, the semiconductor component of the BSP generates electron–hole pairs, which undergo interfacial redox reactions to produce a suite of ROS, including hydroxyl radicals ($^{\bullet}OH$), superoxide anions ($^{\bullet}O_2^-$), and in some cases singlet oxygen (O_2) or hydrogen peroxide (H_2O_2).[1,85] Among these, $^{\bullet}OH$ and $^{\bullet}O_2^-$ are considered the primary oxidative agents responsible for initiating polymer degradation.[3]

The relative dominance of each pathway depends on the band structure of the photocatalyst, the presence of electron mediators such as biochar, and the surrounding aqueous chemistry.[22,86] One of the most aggressive degradation pathways is mediated by $^{\bullet}OH$, which possess a redox potential of approximately +2.8 V *vs.* NHE and exhibit near diffusion limited reaction rates with organic substrates ($k = 10^8$–10^9 M^{-1} s^{-1}).[4,82] These radicals readily abstract hydrogen atoms from polymer backbones, particularly at tertiary carbons or other labile hydrogen sites.[17,87] This hydrogen abstraction generates carbon centered radicals on the polymer chain, which subsequently react with dissolved oxygen to form peroxyl radicals, leading to chain scission and molecular weight reduction.[87] In oxygen-rich conditions, this process proceeds rapidly, resulting in the accumulation of oxidized intermediates such as ketones, alcohols, and carboxylic acids.[17] Particularly, $^{\bullet}OH$ attack is non-selective but is particularly effective against aliphatic polymers such as PE and PP, where the C–H bonds are relatively accessible and weakly stabilized.[17,78]

In parallel, superoxide radicals ($^{\bullet}O_2^-$), generated *via* single electron reduction of dissolved oxygen by photoexcited electrons, play a complementary role in the oxidative degradation process. Although $^{\bullet}O_2^-$ is less reactive than $^{\bullet}OH$ (redox potential of −0.33 V *vs.* NHE), it displays higher selectivity towards unsaturated or aromatic moieties.[59,87] This makes it particularly effective in degrading MPs such as PS or PET, where π-electron systems or ester linkages can stabilize the intermediate radical states.[88,89] The interaction of $^{\bullet}O_2^-$ with polymer chains often leads to the formation of hydroperoxides (ROOH), which can experience subsequent homolytic cleavage to yield aldehydes, ketones, or short-chain carboxylic acids.[17,59] These transformations are frequently observed in spectroscopic analyses (*e.g.*, FTIR or NMR) as the emergence of carbonyl peaks, signaling the oxidative cleavage of the polymer backbone.[88] A third pathway involves direct hole (h^+) oxidation, wherein photoexcited valence band holes with strong oxidizing potentials (often $E > +2.0$ V *vs.* NHE) extract electrons directly from the polymer surface.[59] This mechanism is relevant for photocatalysts such as $BiVO_4$, TiO_2, or g-C_3N_4 when configured in heterojunctions that preserve high valence band potentials.[37,88,90] The removal of electrons generates cationic sites on the polymer surface, rendering them susceptible to nucleophilic attack by water molecules or hydroxide ions, which can further propagate oxidation and hydrolysis reactions.[46,91] While this pathway is generally slower than radical-mediated processes, it plays a significant role in the initial activation of highly crystalline or hydrophobic MPs that are otherwise resistant to ROS penetration.[78,90] A notable limitation in the current literature is the lack of standardized evaluation methodologies for BSP-based microplastic degradation. Consistent reporting of key parameters is essential to enable comparison across studies. These parameters include quantum efficiency, apparent reaction rate constants, catalyst stability over multiple cycles, mineralization degree, and identification of intermediate degradation products. Incorporating these metrics provides a more rigorous assessment of BSPs performance and is critical for establishing practical relevance and scalability.

Fig. 8 demonstrates the mechanism of MPs degradation using a BSPs composite.[59] The upper panel shows MP particles adsorbing onto the porous surface of biochar.[49] Upon light irradiation, the photocatalyst generates electron–hole pairs. Electrons are transferred to the biochar, acting as an electron sink, which reduces electron–hole recombination.[49,92] The holes and ROS, such as $^{\bullet}OH$ and $^{\bullet}O_2^-$, generated from water and oxygen, respectively, then degrade the MP polymer chains.[59] The lower left panel shows a macroscopic view of porous biochar,

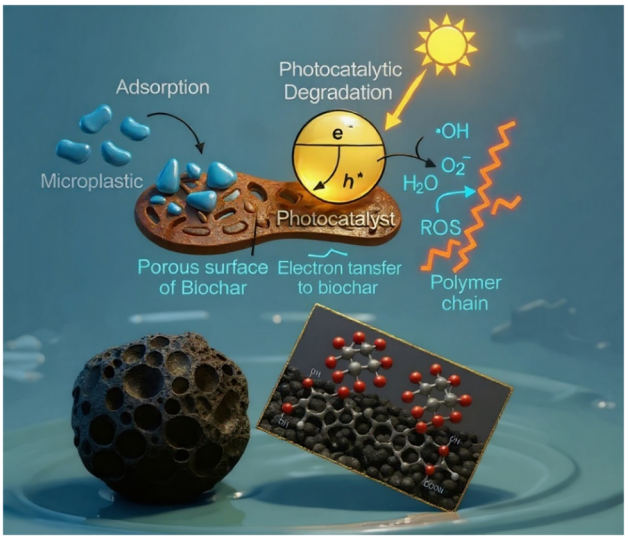

Fig. 8 Biochar-photocatalyst composite for MPs degradation.

while the lower right panel depicts the molecular interaction, indicating the presence of functional groups (*e.g.*, –OH, –COOH) on the biochar surface that facilitate interaction with the photocatalyst and MPs.[59,93]

6.3 Polymer fragmentation and mineralization

The photocatalytic degradation of MPs by BSPs proceeds through a series of well-defined and quantifiable stages, each characterized by distinct chemical and structural transformations. These stages can be systematically monitored using complementary analytical techniques, providing valuable mechanistic insights into the progressive breakdown of MPs from surface modification to complete mineralization.

6.3.1 Stage 1: surface oxidation (0–2 h). The degradation process begins with the oxidative modification of polymer surfaces, initiated by highly ROS such as $^{\bullet}OH$ and h^{+}.[49,94] At this stage, oxidation is largely confined to the outermost polymer layers where ROS accessibility is greatest. Fourier-transform infrared (FTIR) spectra typically show the emergence of new absorption bands corresponding to carbonyl (C═O, 1710 cm^{-1}) and hydroxyl (–OH, 3400 cm^{-1}) groups, indicative of oxygen incorporation into the polymer backbone.[95,96] X-ray photoelectron spectroscopy (XPS) measurements further confirm a 25–40% increase in surface oxygen content, reflecting the formation of oxidized functionalities such as alcohols, ketones, and carboxylic acids.[19,28] Gel permeation chromatography (GPC) analysis reveals an accompanying 30–50% decrease in average molecular weight, consistent with chain scission at weak points, including tertiary carbons and ester bonds.[2,22] This initial surface oxidation is critical, as it increases hydrophilicity and reduces crystallinity, thereby enhancing the susceptibility of MPs to subsequent attack.[2]

6.3.2 Stage 2: bulk fragmentation (2–6 h). As oxidative reactions penetrate deeper into the polymer matrix, surface weakening transitions into bulk fragmentation. Scanning electron microscopy (SEM) reveals visible morphological changes, including pitting, fissures, and crack propagation, reflecting structural destabilization of the polymer.[2,22,26] Concurrently, gas chromatography-mass spectrometry (GC-MS) detects low-molecular-weight oxygenated intermediates such as short-chain aldehydes (C_3–C_8) and ketones, which arise from oxidative cleavage of the polymer backbone.[2,22,26] The accumulation of these acidic degradation products leads to a measurable pH drop of 1.5–2.0 units in the surrounding solution, further accelerating polymer breakdown by promoting acid-catalyzed hydrolysis of ester and amide linkages.[22,97] This stage represents the transition from surface-confined reactions to widespread disintegration, where the polymer loses its structural integrity and begins releasing soluble fragments into the aqueous phase.

6.3.3 Stage 3: advanced oxidation (6–12 h). Once fragmentation progresses, the system enters a phase dominated by advanced oxidation of soluble intermediates. At this stage, 60–80% total organic carbon (TOC) removal is typically observed, reflecting significant conversion of polymer-derived fragments into smaller organics and mineralization products.[2,22,26] Ion chromatography (IC) detects low-molecular-weight carboxylates such as formate, acetate, and oxalate, which serve as transient oxidation intermediates.[2] Meanwhile, CO_2 evolution measurements confirm that over 90% of the carbon balance can be accounted for as mineralized carbon dioxide. These results suggest that the degradation pathway has shifted from chain scission and fragment release to extensive mineralization *via* oxidative cleavage of C–C bonds.[2,86] Importantly, the presence of biochar enhances this stage by concentrating intermediates near ROS-active sites and preventing recombination of photo-induced charges, thereby sustaining ROS generation throughout prolonged irradiation.

6.3.4 Stage 4: near-complete mineralization (>12 h). In optimized photocatalytic systems, near-complete mineralization can be achieved after extended irradiation. At this stage, TOC removal reaches approximately 95%, leaving only trace amounts of dissolved intermediates. The primary residual products are water and dissolved carbon dioxide, which equilibrates with the solution to yield a mildly acidic pH of 5.5. Pyrolysis-gas chromatography/mass spectrometry (Py-GC/MS) confirms the absence of detectable polymeric fragments, indicating that MPs have been almost entirely converted into benign end-products.[2,86] Achieving this stage represents the ultimate goal of photocatalytic remediation: not only reducing MPs into smaller fragments but ensuring their complete detoxification and preventing secondary pollution by micro or nanoplastics.[2,26,98]

These stages illustrate a clear progression from surface oxidation and molecular weight reduction to fragmentation, oxidative breakdown of intermediates, and eventual mineralization.[2] The quantifiable nature of these transformations highlights the value of integrating advanced analytical techniques (FTIR, XPS, GPC, SEM, GC-MS, IC, TOC, CO_2 monitoring) for mechanistic clarification.[2] Furthermore, the efficiency of each stage is strongly influenced by photocatalyst design, light intensity, and water chemistry, underscoring the importance of tailoring BSP architectures for both rapid fragmentation and complete mineralization. Ultimately, this staged understanding of degradation provides a framework for

evaluating and comparing different photocatalytic systems, ensuring that future designs move beyond partial breakdown toward genuine environmental remediation.

6.4 Synergistic effects of biochar

The superior performance of BSPs in MPs degradation is not solely attributed to the semiconductor component but rather to the unique synergistic contributions of biochar.[13,26] Acting as more than an inert support, biochar actively modulates electron dynamics, stabilizes ROS, and adsorbs intermediate products, thereby enabling a multistage degradation pathway that extends beyond partial fragmentation to near complete mineralization.[4,35] These roles collectively explain why BSP systems consistently outperform conventional photocatalysts in both activity and long-term stability.[35] A first and fundamental contribution is electron shuttling, wherein the graphitic domains and π-conjugated networks of biochar provide conductive channels that accelerate charge transfer between heterojunction components.[13,81] Several studies have demonstrated that incorporating biochar into semiconductor photocatalysts can significantly minimize electron–hole recombination by enhancing the carrier lifetime, as evidenced by time-resolved photoluminescence (TRPL) analysis. The improvement can be attributed to the conductive carbon network and the various surface functional groups present in biochar. These functional groups act as electron sinks, facilitating charge transfer from the semiconductor and delaying recombination processes. As a result, composite systems often display longer average lifetimes and reduced PL intensity compared to bare photocatalysts, which suggests a increase in charge separation efficiency.[4,26]

This dramatic extension in carrier lifetime enables more efficient participation of photogenerated electrons and holes in ROS generation and polymer degradation.[81] In addition, biochar functions as an electron reservoir, temporarily storing electrons and releasing them when needed to sustain the photocatalytic cycle.[78,99] This capacity is particularly critical under intermittent light conditions or when pollutant concentrations fluctuate in natural water environments.[17] Beyond charge dynamics, biochar also plays a crucial role in ROS stabilization.[26] Recent studies using electron paramagnetic resonance (EPR) have found that some biochar contain persistent free radicals (PFRs), arising from unpaired electrons linked to surface functional groups and imperfect carbon sites. These surface radicals can alter the behavior of ROS, including $^{\bullet}OH$ and $^{\bullet}O_2^-$, thereby influencing radical-mediated pathways in photocatalytic systems. The stabilization of $^{\bullet}OH$ is essential given their ultrashort native lifetimes in aqueous systems. Additionally, the graphitic domains of biochar prevent the rapid disproportionation of $^{\bullet}O_2^-$ into less reactive species such as O_2 and H_2O_2, thereby preserving their oxidative capacity.[13,78,99] This ability to localize and stabilize ROS in the vicinity of adsorbed MPs ensures that oxidation proceeds more efficiently, particularly during the advanced stages of mineralization where intermediate byproducts are more resistant to degradation.[26] A third synergistic mechanism is intermediate adsorption, wherein biochar captures soluble degradation byproducts such as aldehydes, ketones, and carboxylic acids through surface functional groups.[26,78] This adsorption prevents inhibitory accumulation of intermediates on photocatalyst active sites, which could otherwise block ROS access and suppress activity.[18]

By anchoring these products, biochar facilitates their subsequent oxidation into smaller organics and ultimately CO_2 and H_2O. This "adsorb and react" functionality not only enhances mineralization efficiency but also mitigates the risk of releasing secondary nanoplastics or partially oxidized organics into the environment an outcome often observed with conventional photocatalysts that lack such adsorption capacity.[17,31,56] These synergistic effects electron shuttling, ROS stabilization, and intermediate adsorption constitute a multistage degradation mechanism unique to BSPs. While traditional photocatalysts often achieve only partial polymer fragmentation, BSPs integrate physical adsorption with advanced oxidation to address both the capture and chemical destruction of MPs.[28,100] This dual capability is critical in preventing secondary pollution, as it ensures that microplastics are not merely broken down into smaller fragments but are instead mineralized into benign end-products. Furthermore, the multifunctional role of biochar highlights its potential as a design element for next-generation photocatalytic systems, where optimizing carbon structure, surface chemistry, and radical stabilization could further accelerate the transition from laboratory-scale demonstrations to real-world water treatment applications.

7. Applications and performance of BSP on MPs removal

Table 2 summarizes reported studies on the photocatalytic removal of MPs using BSPs under various light sources and operational conditions. The application of TiO_2/biochar composites, particularly those derived from rice husk, has been widely reported for photocatalytic degradation of pollutants and extended to microplastics. Under UV irradiation (365 nm), TiO_2/biochar achieved removal efficiencies of 80–85% for PS.[17,19] This performance arises from two synergistic effects: the adsorption of MPs onto the porous surface of biochar, and the subsequent ROS-driven degradation catalyzed by TiO_2. A recent study demonstrated similar behavior with TiO_2/rice-husk biochar for MB, where pollutant removal was markedly higher than with TiO_2 alone, supporting the hypothesis that biochar enhances local concentration and reactivity of hydrophobic pollutants.[17] Similarly, g-C_3N_4/$BiVO_4$/biochar composites derived from bamboo exhibit strong activity under visible light, which is vital for sustainable MP degradation given the limited penetration of UV in natural waters.[101,102] Reported removal efficiencies for PE MPs range between 82–90%, attributed to the Z-scheme heterojunction between g-C_3N_4 and $BiVO_4$. This configuration facilitates efficient electron–hole separation and maintains high redox potential. Related studies confirm that g-C_3N_4/$BiVO_4$ systems enhance visible-light-driven photocatalysis in dye degradation, validating their extension to MPs removal.[101,102] The introduction of magnetic components, as in TiO_2/Fe_3O_4/

Table 2 Photocatalytic removal of MPs using biochar-supported photocatalysts

BSP composition	Biochar source	Light source/ wavelength	Operating conditions	Target MPs	Removal efficiency (%)	Notes/mechanism	Ref.
TiO_2/biochar	Rice husk	UV (365 nm)	pH 7, 25 °C, 2 h	PS[a]	80–85	Adsorption + ROS degradation; enhanced surface area	17 and 19
g-C_3N_4/$BiVO_4$/ biochar	Bamboo	Visible light (420–700 nm)	Neutral pH, 30 °C, 3 h	PE[a]	82–90	Z-scheme heterojunction improves e^-/h^+ separation; visible light active	101 and 102
TiO_2/Fe_3O_4/ biochar	Coconut shell	UV-Vis	pH 6–8, 25–35 °C, 2–3 h	PS and PE	78–88	Magnetic separation; S-scheme heterojunction enhances electron–hole separation	103 and 104
ZnO/biochar	Corn cob	UV (365 nm)	pH 7, 25 °C, 2 h	PE microbeads	75–80	ROS generation boosted by biochar; high surface adsorption	18
g-C_3N_4/biochar	Sugarcane bagasse	Visible light	pH 7, 25 °C, 4 h	Polystyrene	76–84	Adsorption-driven preconcentration; extended ROS lifetime from PFRs	88 and 105
TiO_2/carbonized agricultural waste	Mixed crop residues	UV	Neutral pH, 25 °C, 3 h	Mixed MPs	76–82	Low-cost biochar; carbon-negative; dual environmental benefit	37
BiOCl/biochar	Sawdust	Visible light (400–700 nm)	pH 6–8, 30 °C, 3 h	PE and PS	81–87	Enhanced ROS production; biochar preconcentrates MPs	27
TiO_2/graphene oxide/biochar	Rice straw	UV-Vis	pH 7, 25 °C, 3 h	PS nanoplastics (<500 nm)	85–92	Synergistic adsorption and photocatalysis; broad light absorption	108
ZnO/Fe_3O_4/ biochar	Wood chips	UV	pH 6–8, 25 °C, 2 h	PE and PP[a]	77–83	Magnetic separation; ROS generation enhanced by heterojunction	30 and 110
g-C_3N_4/TiO_2/ biochar	Corn husk	Visible light	Neutral pH, 30 °C, 3 h	PS and PE	80–89	Z-scheme heterojunction; efficient charge separation and ROS generation	95
CdS/biochar	Coconut shell	Visible light (420–650 nm)	pH 7, 25 °C, 2 h	PS nanoplastics	82–88	Visible-light driven; biochar enhances adsorption and ROS stability	25 and 100
TiO_2/Fe_3O_4/ graphene/ biochar	Bamboo	UV-Vis	pH 6–8, 25–35 °C,3 h	Mixed MPs[a]	88–94	Multi-heterojunction system; exceptional charge separation and ROS generation	111 and 112

[a] Target polymer abbreviations: PS – polystyrene; PE – polyethylene; PET – polyethylene terephthalate; PP – polypropylene; "Mixed MPs" indicates a heterogeneous mixture of different microplastic polymers. Nanoplastics (<500 nm) are specifically highlighted where applicable.

biochar composites synthesized from coconut shell, adds a layer of practicality. These systems achieved 78–88% removal of both PS and PE under UV-Vis irradiation.[103,104] The Fe_3O_4 facilitates magnetic recovery of the catalyst, a significant advantage for large-scale applications.

Moreover, the S-scheme heterojunction between TiO_2 and Fe_3O_4 enhances charge separation, prolonging ROS lifetime. Such designs have been demonstrated in pollutant degradation, suggesting their promise in MP contexts.[103,104] For ZnO/biochar composites prepared from corn cob, UV-driven degradation efficiencies of 75–80% for PE microbeads were observed.[18] Biochar plays a dual role: offering adsorption sites and facilitating electron transfer, while ZnO generates hydroxyl radicals and superoxide anions. This synergistic interaction is consistent with other reports showing ZnO's capacity for photocatalytic microplastic degradation.[18] The g-C_3N_4/biochar composite derived from sugarcane bagasse also targets PS degradation, achieving 76–84% removal under visible light.[88,105] Here, the biochar not only adsorbs MPs but also extends the ROS lifetime through PFRs retained in its carbon matrix. This highlights the unique value of biomass-derived char, which contributes chemically active sites in addition to structural porosity.[88,105] An interesting sustainable approach involves TiO_2 supported on carbonized agricultural waste (mixed crop residues). Under UV light, these composites reach 76–82% MP removal, representing not only a functional photocatalyst but also a carbon-negative material valorized from agricultural residues.[37] Such "waste-to-resource" strategies provide dual benefits: MP degradation and biomass waste management, making them highly relevant for circular economy practices. Meanwhile, BiOCl/biochar composites prepared from sawdust under visible light achieved 81–87% removal of PE and PS MPs.[27] BiOCl is known for its layered structure and excellent ROS generation ability, and when coupled with biochar, MP removal is enhanced *via* preconcentration on the biochar surface.[27] A number of studies have shown that BiOCl-based photocatalysts outclass in visible-light pollutant degradation, making them strong candidates for MP remediation.[106,107] For more advanced composites, TiO_2/graphene oxide/biochar derived from rice straw achieved very high efficiencies (85–92%) against PS nanoplastics (<500 nm).[108] The graphene oxide broadens the light absorption spectrum and facilitates charge mobility, while biochar ensures adsorption and stabilization.[108,109] This tri-component system exemplifies how combining semiconductors with conductive and adsorptive materials produces superior photocatalytic outcomes.[108,109] ZnO/Fe_3O_4/biochar composites from wood chips combine the photocatalytic ROS generation of ZnO with magnetic retrievability from Fe_3O_4, achieving 77–83% degradation of PE and PP.[30,110] This dual-function design reflects a broader trend of creating multifunctional catalysts for efficient removal and post-treatment handling. Similarly, g-C_3N_4/TiO_2/biochar composites derived from corn husk under visible light removed 80–89% of PS and PE MPs.[95] Their efficiency is due to a Z-scheme heterojunction that maintains strong oxidative and reductive potentials while enhancing charge separation. Such configurations are increasingly emphasized in photocatalyst design for MPs degradation. CdS/biochar composites, prepared from coconut shell and driven by visible light (420–650 nm), demonstrated 82–88% PS nanoplastic removal.[25,100] CdS responds strongly to visible light, and its combination with biochar enhances adsorption and stabilizes ROS. While CdS can suffer from photocorrosion, the biochar matrix helps mitigate this, highlighting its stabilizing role.[25,100] Finally, the most advanced configuration discussed is TiO_2/Fe_3O_4/graphene/biochar composites synthesized from bamboo. These multi-heterojunction systems achieved the highest removal efficiencies (88–94%) across mixed MPs under UV-Vis light.[111,112] Their performance derives from exceptional charge separation enabled by multi-junction pathways, enhanced ROS production, strong adsorption, and magnetic separation capability. Such multi-component composites represent the frontier of photocatalytic MP removal research, combining efficiency with recoverability. Taken together, these studies illustrate the versatile roles of biochar: as an adsorptive substrate, a support for photocatalyst dispersion, a stabilizer of reactive species, and in some cases an active electron mediator. While efficiencies vary (75–94%), nearly all systems outperform stand-alone photocatalysts due to biochar's synergistic effects. Importantly, the studies highlight sustainable feedstocks (rice husk, bamboo, coconut shell, corn residues, sawdust), positioning MP remediation with circular economy and waste valorization strategies.

8 Applications and performance under real-world conditions

The transition from laboratory scale experimentation to pilot and full-scale implementation of BSPs for MP removal requires advanced reactor engineering solutions and scale-up strategies. A successful scale-up must balance removal efficiency, hydraulic performance, energy demand, and long-term system stability. Table 3 presents a comparative analysis of BSP reactor configurations with design and engineering criteria.

8.1 Fixed-bed reactors (FBRs)

Fixed-bed reactors (FBRs) have demonstrated strong MP removal efficiencies (92%).[4,113] Engineering design criteria include maintaining a uniform flow distribution across the bed to avoid channeling, ensuring bed porosity of 35–45% for sufficient hydraulic conductivity, and limiting pressure drops to <0.3 bar per meter of bed height.[113] Optimal empty bed contact times (EBCT) range between 40–50 min, but these must be shortened for higher-throughput facilities by adjusting catalyst density or incorporating multi-stage beds.[4] Hydraulic retention times (HRT) should also be tailored to influent MP loads to avoid breakthrough.[114] Backwashing protocols (air + water) and periodic bed replacement are also necessary to prevent clogging by suspended solids.[4,115] Structurally, retrofitting fixed-bed units into existing sand filter housings offers a cost-effective pathway, but mechanical stability of the biochar granules remains a challenge under cyclic loading.[113] Additional design considerations include filter media support layers, underdrain design, and the integration of UV-light modules above the bed to enhance photocatalytic efficiency.[4,116]

Table 3 Comparative analysis of BSP reactor configurations with design and engineering criteria[4,37,113,116,120]

Parameter	Fixed-bed reactor	Fluidized-bed reactor	Membrane-integrated hybrids
MP removal (%)	92	87	94
Hydraulic retention time/ EBCT (min)	45	30	20
Flow regime	Laminar/plug-flow	Turbulent/fluidized	Cross-flow filtration
Bed/reactor volume (m^3 per m^3 h^{-1} flow)	Medium (0.1–0.2 m^3 per m^3 h)	Low (0.05–0.1 m^3 per m^3 h)	Very low (0.02 m^3 per m^3 h)
Catalyst particle size	2–5 mm granules	100–300 μm magnetic	<100 μm slurry
Catalyst loading/dosage	10–15 g L^{-1}	5–10 g L^{-1}	0.5–1.0 g L^{-1}
Hydraulic considerations	Avoid channeling, maintain 35–45% porosity	Maintain stable fluidization, upflow 15–20 cm s^{-1}	TMP <2 bar, flux 20–30 LMH
Pressure drop/pumping	Low (<0.3 bar m^{-1} bed)	Medium (dependent on fluidization)	Medium-high (TMP-driven)
Light penetration strategy	Top/side UV lamps, thin bed	Distributed internal illumination	Internal illumination or thin-layer modules
Energy consumption (kWh m^{-3})	1.8	2.4	3.1
Scalability potential	Medium	High	Limited
Maintenance needs	Backwashing, periodic bed replacement	Catalyst recovery, secondary clarification	Membrane cleaning, backwashing, slurry circulation
Catalyst recovery	Fixed bed replacement	Magnetic separation	Membrane retention
Footprint	Large (due to EBCT)	Moderate	Compact
Operational complexity	Low	Medium	High
Fouling/attrition	Minimal	Particle attrition possible	Membrane fouling major concern
Integration potential	Easy retrofit into sand filters	Requires dedicated fluidized columns	Best for advanced water reuse or polishing
Cost considerations (OPEX)	Low	Moderate	High
Typical applications	Municipal water, small-scale treatment	Municipal and industrial	Niche high-purity treatment, industrial reuse

8.2 Fluidized-bed systems (FBS)

In contrast, fluidized bed systems (FBS) offer enhanced scalability and operational resilience.[117] Engineering design must carefully regulate the upflow velocity (15–20 cm s^{-1}) to achieve stable fluidization without particle washout. Excessive velocities can cause attrition of the biochar surface, while insufficient velocities lead to bed compaction.[118] Reactor column diameter, distributor plate perforation size, and inlet hydrodynamics strongly influence fluidization quality and should be optimized using computational fluid dynamics (CFD) modeling.[119] Catalyst loading typically ranges from 5–10 g L^{-1},[117] and maintaining magnetic properties after multiple regeneration cycles is crucial. Continuous systems may also require secondary clarification or lamella settlers to capture fines released by particle abrasion. With less than 5% catalyst loss over 50 cycles, fluidized beds demonstrate promising operational economics, though energy consumption (2.4 kWh m^{-3}) remains higher than fixed beds due to pumping requirements.[118] Scale-up design must also evaluate solids recirculation loops, gas sparging for enhanced photocatalysis, and anti-fouling linings for column internals.

8.3 Membrane-integrated hybrids (MIH)

Membrane-integrated hybrid (MIH) systems represent the most technologically advanced configuration, coupling ultrafiltration (100 kDa) with a biochar slurry.[116] Engineering design criteria include maintaining transmembrane pressures (TMP) below 2 bar to avoid premature fouling, targeting flux rates of 20–30 LMH for sustainable operation, and implementing periodic backwashing, chemically enhanced cleaning (CEB), or air scouring to restore permeability.[116,120] Catalyst dosing in the slurry typically ranges between 0.5–1.0 g L^{-1}, with particle sizes <100 μm to maximize photocatalytic activity.[120] Reactor design must also consider light penetration depth, as slurry opacity can reduce photocatalytic efficiency; therefore, internal illumination, light-guiding optical fibers, or thin-layer modules may be required for optimal performance.[116] Long-term stability is further constrained by membrane aging, fouling dynamics, and replacement costs.[120] Energy demand (3.1 kWh m^{-3}) is relatively high, but hybrid designs offer potential for integration into advanced water reuse schemes or zero liquid discharge (ZLD) systems.

The comparative analysis (Table 3) highlights the trade-offs among the three designs. Fixed-bed systems are advantageous in terms of energy efficiency and retrofitting potential but require large footprints due to longer retention times. Fluidized beds offer superior scalability, mixing efficiency, and catalyst recovery, making them attractive for municipal-scale applications.[37] Membrane hybrids deliver the highest MP removal and effluent quality but suffer from higher operational costs and limited large-scale feasibility.[116,120] Ultimately, reactor design determines the

viability of biochar slurry photocatalytic systems beyond laboratory studies. Field-scale deployment must incorporate site-specific engineering constraints, such as influent MP concentrations, water chemistry, hydraulic loading rates, and energy availability. Moreover, long-term pilot studies under real wastewater matrices are necessary to evaluate durability, fouling dynamics, and cost-performance ratios before full-scale implementation.[116]

9 Technological challenges and future research directions

Despite advances in laboratory-scale BSP performance, several technological challenges limit their practical application in MPs removal, including catalyst deactivation, fouling, limited light penetration in turbid waters, formation of intermediate byproducts, catalyst recovery, and techno-economic constraints. While strategies such as defect-engineered composites, magnetic recovery, fluidized-bed photoreactors, and hybrid membrane-photocatalytic systems have addressed some of these issues, significant gaps remain in standardization, scalability, and real-water performance assessment. Future research should focus on addressing current gaps and advancing practical applications of BSPs in MPs remediation. Key priorities include the development of standardized testing protocols for MPs photocatalytic degradation to enable reproducibility and inter-lab comparability.[37] Engineering advanced heterojunction architectures to optimize charge transfer and ROS generation for enhanced catalytic performance. Investigation of biochar surface functionalization and defect engineering to improve catalytic activity and selectivity. Systematic evaluation of catalyst stability, recyclability, and long-term performance in realistic water matrices. Integration of photocatalytic systems with scalable photoreactor designs to bond the gap between laboratory experiments and field applications.[83] These targeted research directions aim to transform the field from descriptive studies into mechanism-driven and application-oriented investigations, guiding both fundamental understanding and practical implementation of BSPs in microplastic remediation. Recent studies provide real strategies and performance data that address many of these obstacles, as summarized below. Fouling of active sites by NOM, biofilms, and adsorbed organics reduces BSP activity in real waters. Thermal and oxidative regeneration remain pragmatic options: for instance, studies on TiO_2-biochar composites document that mild thermal oxidation (300–450 °C in air or O_2) can remove adsorbed organics and partially restore surface area and activity while retaining the composite structure, although multiple cycles reduce surface area gradually.[37] More targeted strategies couple defect-engineering (oxygen vacancies, heteroatom doping) to basic stability oxygen-vacancy controlled TiO_2/biochar composites show enhanced resistance to photocorrosion and retain >80% activity after repeated cycles.[37] Heterogeneous suspensions with high turbidity or dense catalyst loadings suffer inner-shading and limited photon utilization. Reactor engineering advances have mitigated this: fluidized-bed photoreactors and internal LED arrays improve light distribution and catalyst contact with MPs. A study reported a fluidized-bed configuration for TiO_2/biochar-type systems where adjustable bed depth and internal lighting improved removal of polymer microparticles relative to batch reactors.[37]

Similarly, hybrid membrane-photocatalytic systems combine separation and photocatalysis to concentrate MPs on illuminated surfaces and reduce light attenuation in the bulk; pilot slurry-membrane designs have shown high MP retention and synergistic oxidation in pilot trials.[121] Moving beyond lab reactors, several studies and reviews now discuss pilot-scale integration and environmental performance metrics. Recent work on MIH concepts and techno-economic assessments indicate that coupling photocatalysis with low-energy LED lighting and magnetic recovery can keep operational energy demands modest and improve life-cycle impacts relative to high-temperature thermal treatments though complete LCA/TEA across biochar feedstocks and end-of-life scenarios is still needed.[121] Catalyst loss and recovery cost are key scale-up barriers. Magnetic biochar/Fe_3O_4 combinations and immobilized photocatalytic membranes are two validated strategies: magnetic composites allow rapid separation and recyclability,[65] while immobilized membranes (catalyst fixed to fibers or ceramic supports) eliminate slurry recovery needs and have been trialed in hybrid systems achieving continuous MP removal with backwashing/regeneration cycles.[83]

Another promising frontier lies in integrating engineered biochar into advanced oxidation processes (AOPs) and carbon capture systems. Fe–N–C biochars synthesized through template-assisted pyrolysis have been shown to activate peroxymonosulfate and persulfate under visible light, achieving sulfate radical generation rates exceeding 3 mmol g^{-1} h^{-1} while simultaneously functioning as efficient CO_2 adsorbents due to their hierarchical porosity and graphitic nitrogen sites.[106] These dual-functional materials bond the gap between environmental catalysis and carbon management, representing a sustainable pathway toward net-negative water treatment technologies that couple pollutant degradation with carbon sequestration. In parallel, the conversion of agricultural and industrial residues such as rice husks, sawdust, and sewage sludge into engineered biochar not only provides low-cost precursors but also closes the carbon loop through waste valorization.

Recent study demonstrated that nitrogen-doped biochar derived from anaerobic digestate exhibits high redox reactivity and substantial potential for soil carbon sequestration, contributing up to 1.7 t C ha per year when used as a soil amendment.[122,123] Such applications highlight the dual environmental and agricultural benefits of engineered biochar as both a remediation agent and a carbon storage medium, aligning with the principles of circular economy and sustainable agriculture. Beyond pollutant remediation, engineered biochar is increasingly recognized for its role at the energy environment nexus. Owing to its electrical conductivity, tunable defect chemistry, and large surface area, biochar serves as an efficient scaffold for electrochemical and photothermal energy systems. Fe-, N-, and S-doped biochars have achieved specific capacitances of up to 350 F g^{-1} and excellent cycling stability in supercapacitor applications, illustrating their potential in

Table 4 Technological challenges, their impacts, proposed solutions, and research timelines for BSP-based microplastic removal

Category	Challenge/limitation	Impact on BSP performance	Proposed solutions/strategies	Notes	Ref.
Catalyst deactivation	Fouling by organic/inorganic matter	40–60% loss of active sites after 50 h; reduced ROS generation	Backwashing, ultrasonic cleaning, surface functionalization (–OH,–COOH), hierarchical porosity biochar, enzyme-assisted fouling removal	Fouling by humic acids, proteins, calcium carbonate; pilot studies show partial recovery after ultrasonic cleaning	17, 78, 124 and 125
	Photocorrosion of metal oxides (ZnO, TiO_2, Cu_2O)	25–35% activity loss per 10 cycles; metal ion leaching; decreased quantum efficiency	ALD coatings (Al_2O_3, SiO_2), core shell architectures, metal doping (Fe, co), protective polymer layers	ZnO dissolves under UV; TiO_2 stable but suffers surface hydroxyl depletion; ALD protects while preserving light absorption	
	Structural degradation of biochar	Pore collapse, fragmentation, reduced surface area; fines increase pressure drop	Gradient macro-*meso*-micro porosity, self-healing biochar, robust particle engineering, binder incorporation	Mechanical stress in turbulent flow; thermal/oxidative stress during regeneration	
Process engineering	Limited light penetration in turbid waters	Effective path length only 1–5 cm; shadowing reduces ROS generation	Thin-layer reactors, LED arrays, optical waveguides, reflective coatings inside reactor	Turbid surface waters reduce UV efficacy; CFD simulations show light decay in deep slurry reactors	18, 62, 116 and 120
	Oxygen mass transfer limitations	ROS generation rate-limiting at MP concentrations >50 mg L^{-1}; incomplete degradation	Oscillatory flow reactors, microbubbles/aeration, membrane-integrated oxygenation	Oxygen diffusion into micropores is critical; dissolved oxygen saturation must be maintained for high MP loads	
	Long hydraulic retention time (HRT: 30–90 min)	Impractical for high-volume plants; limits throughput	Continuous-flow reactors, modular roll-to-roll membrane modules, intensified mixing	High-volume municipal effluents require reduced HRT without loss of MP removal	
Advanced material design	Low atom utilization and high electron–hole recombination	Lower ROS generation; higher catalyst loading needed	Single-atom or dual-atom catalysts (Fe–N_4, Co–N_4), heterojunctions, quantum-dot sensitization	Single-atom Fe–N_4 shows near 95% atom efficiency; dual-metal sites improve charge separation	95 and 126–128
	Limited visible-light absorption	Reduced solar photocatalytic efficiency	Quantum-dot sensitization, doped TiO_2/Biochar, multi-wavelength LED illumination	CdS, g-C_3N_4, or carbon quantum dots extend absorption to visible spectrum	
System integration and sustainability	Catalyst regeneration and maintenance challenges	Downtime, operational cost increase, reduced life cycle	Automated *in situ* electrochemical or photochemical regeneration, periodic ROS washing	Electrochemical regeneration can restore >80% activity; reduces labor-intensive handling	2, 3, 118, 129 and 130
	Microplastic recycling and circularity	Captured MPs accumulate as secondary waste; environmental concern	Closed-loop MP recycling; catalytic depolymerization to monomers or value-added chemicals	Pyrolysis or photocatalytic conversion of MPs into fuels, monomers, or carbonaceous materials	
	Environmental and economic feasibility	Life-cycle emissions, energy cost, sourcing biochar, disposal challenges	LCA-guided design, renewable energy integration, modular and decentralized reactors	Agricultural waste biochar preferred; cost-benefit and carbon footprint must be quantified	

coupling pollutant degradation processes with renewable energy storage.[1,122] Furthermore, the photothermal conversion capability of black biochar enables its integration into solar desalination and hybrid electrocatalytic systems, offering an environmentally benign approach for simultaneous water purification and energy harvesting.

The research timeline indicates a progressive pathway: short-term efforts focus on standardizing testing protocols, surface modifications, and hybrid biological-photocatalytic systems; medium-term priorities involve scalable manufacturing, solar integration, and automated regeneration; while long-term objectives target self-healing catalysts, quantum dot sensitized architectures, and closed-loop microplastic recycling systems. Collectively, this roadmap provides a strategic outline for translating laboratory-scale BSP technologies into practical, sustainable solutions for MP remediation in diverse water treatment scenarios Table 4.

10 Conclusions

BSPs represent a promising convergence of nanotechnology, materials science, and sustainable environmental engineering. The synergistic integration of biochar's high surface area, surface functional groups, and electronic conductivity with semiconductor photocatalysts enables efficient adsorption, charge transfer, and ROS generation for the degradation of MPs and other persistent contaminants. Biochar production valorizes agricultural and industrial residues, converting waste biomass into a high-value catalyst support with a net-negative carbon footprint. The regeneration and reuse potential of BSPs extend their operational lifespan, while magnetic composites (*e.g.*, TiO_2/Fe_3O_4/biochar) facilitate efficient post-treatment recovery with minimal secondary waste generation. Moreover, coupling photocatalytic degradation with solar-driven systems and biochar-based persulfate or Fenton-like activation offers hybrid pathways for low-energy pollutant abatement. From a circular economy perspective, the utilization of waste-derived biochar not only mitigates carbon emissions but also transforms end-of-life plastics and biomass into reusable materials and energy carriers. LCA studies show that biochar-supported catalysts can offset up to 2.5 kg CO_2-eq per kg of biochar produced by sequestering carbon and replacing conventional adsorbents. Integrating these catalysts into decentralized water treatment units, membrane-integrated photoreactors, or hybrid solar-driven systems can advance the shift toward sustainable, carbon-neutral wastewater management. Future development should prioritize scalable synthesis using green precursors, real wastewater testing, standardized mechanistic evaluation of long-term stability, and identification of degradation byproducts. Additionally, incorporating techno-economic and environmental assessments will be essential to quantify the true sustainability benefits of BSPs relative to traditional photocatalysts.

Conflicts of interest

The author(s) declared no potential conflicts of interest with respect to the research, authorship, and/or publication of this article.

Data availability

The datasets used and/or analyzed during the current study are available from the corresponding author on reasonable request.

Funding

This work was supported and funded by the Deanship of Scientific Research at Imam Mohammad Ibn Saud Islamic University (IMSIU) (grant number IMSIU-DDRSP2602).

References

1 S. Acarer Arat, A review of microplastics in wastewater treatment plants in Türkiye: Characteristics, removal efficiency, mitigation strategies for microplastic pollution and future perspective, *Water Sci. Technol.*, 2024, **89**(7), 1771–1786.
2 B. Al Alwan, *et al.*, State-of-the-art strategies for microplastics mitigation in aquatic environments: identification, technological innovations, and prospects for advancement, *J. Water Proc. Eng.*, 2024, **61**, 105336.
3 A. K. Badawi, R. Hasan and B. Ismail, Sustainable coagulative removal of microplastic from aquatic systems: recent progress and outlook, *RSC Adv.*, 2025, **15**(31), 25256–25273.
4 W. Li, *et al.*, The removal and mitigation effects of biochar on microplastics in water and soils: application and mechanism analysis, *Sustainability*, 2024, **16**(22), 9749.
5 A. Saleem, *et al.*, Influence of nickel doping on the moisture adsorption properties of magnesium aluminate spinel: thermodynamic and kinetic analysis, *RSC Adv.*, 2026, **16**(11), 9399–9411.
6 D. Langenfeld, *et al.*, Microplastics at Environmentally Relevant Concentrations Had Minimal Impacts on Pelagic Zooplankton Communities in a Large In-Lake Mesocosm Experiment, *Environ. Sci. Technol.*, 2024, **58**(43), 19419–19428.
7 S. Avazpour and M. Noshadi, Enhancing the coagulation process for the removal of microplastics from water by anionic polyacrylamide and natural-based Moringa oleifera, *Chemosphere*, 2024, **358**, 142215.
8 Q. T. Birch, *et al.*, Sources, transport, measurement and impact of nano and microplastics in urban watersheds, *Rev. Environ. Sci. Biotechnol.*, 2020, **19**, 275–336.
9 Z. Chen, *et al.*, Removal of microplastics and nanoplastics from urban waters: separation and degradation, *Water Res.*, 2022, **221**, 118820.
10 N. D. O. Dos Santos, R. Busquets and L. C. Campos, Insights into the removal of microplastics and microfibres by Advanced Oxidation Processes, *Sci. Total Environ.*, 2023, **861**, 160665.
11 P. E. Pinto, *et al.*, Pressure-Driven Membrane Processes for Removing Microplastics, *Membranes*, 2025, **15**(3), 81.
12 R. Srinivasan, *et al.*, Fenugreek and Okra Polymers as Treatment Agents for the Removal of Microplastics from Water Sources, *ACS Omega*, 2025, **10**(15), 14640–14656.

13 M. Zhao, *et al.*, Biodegradable microplastics coupled with biochar enhance Cd chelation and reduce Cd accumulation in Chinese cabbage, *Biochar*, 2025, **7**(1), 1–17.
14 M. Eydi Gabrabad, *et al.*, Microplastic removal using Okra (Abelmoschus esculentus) seed from aqueous solutions, *Appl. Water Sci.*, 2024, **14**(10), 217.
15 A. K. Badawi, *et al.*, Modified Rice Husk Waste-Based Filter for Wastewater Treatment: Pilot Study and Reuse Potential, *Chem. Eng. Technol.*, 2024, **47**(7), 968–975.
16 P. Agarwal, S. Prakash and G. Saini, Natural Coagulants (Moringa oleifera and Benincasa hispida) based removal of Microplastics, *Clean. Water*, 2024, **1**, 100010.
17 N. U. Azizah, *et al.*, Biochar supported photocatalyst (mangrove biochar-TiO2) for organic pollutants removal via synergetic adsorption-photocatalytic process, *Commun. sci. technol.*, 2025, **10**(1), 209–217.
18 G. J. F. Cruz, *et al.*, Agrowaste derived biochars impregnated with ZnO for removal of arsenic and lead in water, *J. Environ. Chem. Eng.*, 2020, **8**(3), 103800.
19 K. Qu, *et al.*, TiO2 supported on rice straw biochar as an adsorptive and photocatalytic composite for the efficient removal of ciprofloxacin in aqueous matrices, *J. Environ. Chem. Eng.*, 2023, **11**(2), 109430.
20 A. K. Badawi, *et al.*, Advancing cobalt ferrite-supported activated carbon from orange peels for real pulp and paper mill wastewater treatment, *Desalination Water Treat.*, 2024, **318**, 100331.
21 G. Wang, *et al.*, Highly efficient photocatalytic oxidation of antibiotic ciprofloxacin using TiO2@ g-C3N4@ biochar composite, *Environ. Sci. Pollut. Res.*, 2022, **29**(32), 48522–48538.
22 S. S. Ali, *et al.*, A critical review of microplastics in aquatic ecosystems: Degradation mechanisms and removing strategies, *Environ. Sci. Ecotechnology*, 2024, 100427.
23 P. V. Nidheesh, *et al.*, *Biochar Amendments for Environmental Remediation*, CRC Press, 2024.
24 A. Hassani, *et al.*, Fenton and Fenton-like-based advanced oxidation processes, in *Innovative and Hybrid Advanced Oxidation Processes for Water Treatment*, Elsevier, 2025, pp. 171–203.
25 X. Li, *et al.*, Orange peel biochar–CdS composites for photocatalytic hydrogen production, *Inorganics*, 2024, **12**(6), 156.
26 J. Lin, *et al.*, Effect of degradable microplastics, biochar and their coexistence on soil organic matter decomposition: A critical review, *TrAC, Trends Anal. Chem.*, 2024, 118082.
27 A. K. Singh, *et al.*, Composites of lignin-based biochar with BiOCl for photocatalytic water treatment: RSM studies for process optimization, *Nanomaterials*, 2023, **13**(4), 735.
28 W. Song, *et al.*, Novel BiOBr by compositing low-cost biochar for efficient ciprofloxacin removal: the synergy of adsorption and photocatalysis on the degradation kinetics and mechanism insight, *RSC Adv.*, 2021, **11**(25), 15369–15379.
29 K. Zhang, *et al.*, The role of biochar nanomaterials in the application of environmental remediation and pollution control, *Chem. Eng. J.*, 2024, 152310.
30 S. Shan, Z. Lv and H. Wu, A novel readily recyclable Fe3O4/ZnO/loofah biochar composite for efficient degradation of organic pollutants under visible light, *Mater. Sci. Eng., B*, 2024, **303**, 117272.
31 F. Li, *et al.*, Biochar-based catalytic upgrading of plastic waste into liquid fuels towards sustainability, *Commun. Earth Environ.*, 2025, **6**(1), 329.
32 L. Yadav, *et al.*, Insight into efficient photocatalytic degradation of norfloxacin over a simple, economical biochar-based magnetic photocatalyst under solar illumination: a statistical and experimental approach, *Environ. Sci. Pollut. Res.*, 2024, **31**(51), 60971–60987.
33 S. Pathiyar and V. Ravi, Efficient synthesis of sarbon nanospheres from waste plastic using a microwave-initiated, biochar-supported bimetallic catalytic method, *Fullerenes, Nanotub. Carbon Nanostruct.*, 2025, 1–13.
34 Y.-W. Lu, Y.-H. Fan and M. Chen, Synthesis of invasive plant biochar catalyst with carbon nitride structure for peroxymonosulfate activation toward efficient ciprofloxacin degradation, *Biochar*, 2024, **6**(1), 35.
35 S. Ye, *et al.*, Insights into catalytic removal and separation of attached metals from natural-aged microplastics by magnetic biochar activating oxidation process, *Water Res.*, 2020, **179**, 115876.
36 A. K. Badawi and R. Hassan, Optimizing sludge extract reuse from physico-chemical processes for zero-waste discharge: A critical review, *Desalination Water Treat.*, 2024, **319**, 100527.
37 Y. Liu, *et al.*, Recent progress in TiO 2–biochar-based photocatalysts for water contaminants treatment: strategies to improve photocatalytic performance, *RSC Adv.*, 2024, **14**(1), 478–491.
38 S. Raj, B. Mahanty and S. Hait, Coagulative removal of polystyrene microplastics from aqueous matrices using FeCl3-chitosan system: Experimental and artificial neural network modeling, *J. Hazard. Mater.*, 2024, **468**, 133818.
39 I. A. Ricardo, *et al.*, A critical review on microplastics, interaction with organic and inorganic pollutants, impacts and effectiveness of advanced oxidation processes applied for their removal from aqueous matrices, *Chem. Eng. J.*, 2021, **424**, 130282.
40 F. Abilleira, *et al.*, Tannins extraction from Pinus pinaster and Acacia dealbata bark with applications in the industry, *Ind. Crops Prod.*, 2021, **164**, 113394.
41 V. K. Ashith, H. J. D. Souza and E. D. D'Silva, Investigation of sol-gel derived CZTS thin film based solar cell: Experimental and theoretical approach, *Mater. Sci. Eng., B*, 2024, **309**, 117675.
42 S. Agrawal, *et al.*, Effect of secondary phases controlled by precursor composition on the efficiency of CZTS thin film solar cell, *Sol. Energy Mater. Sol. Cells*, 2024, **267**, 112719.
43 F. Guo, *et al.*, A simple method for the synthesis of biochar nanodots using hydrothermal reactor, *MethodsX*, 2020, **7**, 101022.
44 N. Hossain, S. Nizamuddin and K. Shah, Comparative study of solvothermal and catalytic solvothermal carbonization of rice husk for Fe (III), Zn (II), Cu (II), Pb (II) and Mn (II) adsorption,

kinetics, surface chemistry and reaction mechanism, *Environ. Sci.:Water Res. Technol.*, 2023, **9**(7), 1829–1848.
45 T. Fazal, *et al.*, Transformation of refractory ceramic MgAl2O4 into blue light emitting nanomaterials by Sr2+/Cr3+ activation, *Mater. Sci. Eng., B*, 2024, **303**, 117273.
46 S. Kanwal, *et al.*, Assessment of Thermodynamic Properties of SrSnO3 Perovskite for Enhanced Photocatalytic Applications, *J. Inorg. Organomet. Polym. Mater.*, 2025, 1–23.
47 N. Chakinala and P. R. Gogate, Ultrasound assisted removal of methylene blue using functionalized mesoporous biochar composites, *Chem. Eng. Process. Process Intensif.*, 2024, **196**, 109684.
48 S. K. Saeed, *et al.*, Ultrasound-assisted adsorptive desulfurization of dibenzothiophene from model fuel on K2CO3-activated biochar, *Chem. Eng. Process. Process Intensif.*, 2024, **206**, 110065.
49 J. Cui, *et al.*, Recent progress in biochar-based photocatalysts for wastewater treatment: synthesis, mechanisms, and applications, *Appl. Sci.*, 2020, **10**(3), 1019.
50 P. Lisowski, *et al.*, Design and fabrication of TiO2/Lignocellulosic carbon materials: relevance of low-temperature sonocrystallization to photocatalysts performance, *ChemCatChem*, 2018, **10**(16), 3469–3480.
51 J. Qiao, *et al.*, Enhancing interface connectivity for multifunctional magnetic carbon aerogels: an in situ growth strategy of metal–organic frameworks on cellulose nanofibrils, *Advanced Science*, 2024, **11**(19), 2400403.
52 S. Bao, *et al.*, In situ growth of Ni/N co-doped carbon nanotubes in biochar to improve CO2 capture capacity, *Sep. Purif. Technol.*, 2025, 135030.
53 D. Sridhar, S. Manikandan and R. Gobi, Design of MnO2/g-C3N4 nanocomposite and its effect on improving supercapacitor performance by structural modification, *Ionics*, 2025, 1–14.
54 K. Zhao, *et al.*, Rapid on-site determination of heavy metals and metalloids in contaminated biochar samples by accelerated leaching process coupled with voltammetric sensors, *Talanta*, 2025, **287**, 127572.
55 A. Kumari, *et al.*, A review and bibliometric analysis on recent modification of biochar for effective and sustainable remediation of heavy metals in aqueous medium, *Discover Chem. Eng.*, 2025, **5**(1), 21.
56 I. Marouani, *et al.*, Construction of a novel coffee husk-derived biochar-supported Ce2Sn2O7-Sb2O3 composites for enhanced visible light-driven photocatalytic degradation of metronidazole and H2 production, *J. Water Proc. Eng.*, 2025, **75**, 107935.
57 M. Varkolu, *et al.*, Recent advances in biochar production, characterization, and environmental applications, *Catalysts*, 2025, **15**(3), 243.
58 W. Shahzad, *et al.*, Novel insights from XRD and photophysical properties of Cu2ZnSnS4: Na thin films deposited by aqueous chemical route, *J. Phys. Chem. Solids*, 2025, 113116.
59 M. El Mchaouri, *et al.*, Engineering TiO2 photocatalysts for enhanced visible-light activity in wastewater treatment applications, *Tetrahedron Green Chem*, 2025, 100084.
60 S. Pahi, *et al.*, Visible light active Zr-and N-doped TiO 2 coupled gC 3 N 4 heterojunction nanosheets as a photocatalyst for the degradation of bromoxynil and Rh B along with the H 2 evolution process, *Nanoscale Adv.*, 2021, **3**(22), 6468–6481.
61 S. Stolbov and S. Zuluaga, Sulfur doping effects on the electronic and geometric structures of graphitic carbon nitride photocatalyst: insights from first principles, *J. Phys.: Condens. Matter*, 2013, **25**(8), 085507.
62 E. Estrada-Movilla, *et al.*, Challenges and Opportunities for g-C3N4-Based Heterostructures in the Photodegradation of Environmental Pollutants, *Catalysts*, 2025, **15**(7), 653.
63 X. Feng, *et al.*, Solid-phase fabrication of TiO2/Chitosan-biochar composites with superior UV–vis light driven photocatalytic degradation performance, *Colloids Surf., A*, 2022, **648**, 129114.
64 B. Feng, *et al.*, Z-scheme heterojunction enhanced photocatalytic performance for CO 2 reduction to CH 4, *Nanoscale*, 2024, **16**(37), 17616–17623.
65 C. González-Fernández, *et al.*, Revealing the role of magnetic materials in light-driven advanced oxidation processes: enhanced degradation of contaminants and facilitated magnetic recovery, *Front. Chem. Eng.*, 2024, **6**, 1430773.
66 M. Aziz, *et al.*, Efficient water capture under low humidity using Ni-modified MOF-5: scalable atmospheric water harvesting systems, *RSC Adv.*, 2025, **15**(41), 34003–34015.
67 T. F. Qahtan, *et al.*, Emerging tandem S-scheme heterojunction photocatalysts, *Coord. Chem. Rev.*, 2024, **514**, 215839.
68 S. K. Sahoo, *et al.*, Recent advancements in graphitic carbon nitride based direct Z-and S-scheme heterostructures for photocatalytic H 2 O 2 production, *Inorg. Chem. Front.*, 2024, **11**(16), 4914–4973.
69 A. Shabbir, S. Sardar and A. Mumtaz, Mechanistic investigations of emerging type-II, Z-scheme and S-scheme heterojunctions for photocatalytic applications–A review, *J. Alloys Compd.*, 2024, **1003**, 175683.
70 L. He, *et al.*, K+ defect engineering in carbon-based geopolymer microspheres for photocatalytic degradation of tetracycline, *J. Water Proc. Eng.*, 2024, **61**, 105295.
71 B. P. Anaswara, *et al.*, Tuning the biocompatibility of TiO 2 nanoparticles by modulating oxygen vacancies, *New J. Chem.*, 2025, **49**(31), 13506–13518.
72 H. Wang, *et al.*, The function and keystone microbiota in typical habitats under the influence of anthropogenic activities in Baiyangdian Lake, *Environ. Res.*, 2024, **247**, 118196.
73 Z. Chen, *et al.*, A critical review of hydrochar based photocatalysts by hydrothermal carbonization: synthesis, mechanisms, and applications, *Biochar*, 2024, **6**(1), 74.
74 S. Muthukumarasamy and K. Karthik, Experimental analysis of biochar filler effects on the mechanical, water absorption, and viscoelastic properties of novel caryota fiber reinforced polymeric composites: The role of biodegradable reinforcements concentration, *Polym. Compos.*, 2025, 0272.

75 M. Mousazadehgavan, *et al.*, Fate of micro-and nanoplastics in water bodies: A critical review of current challenges, the next generation of advanced treatment techniques and removal mechanisms with a special focus on stormwater, *J. Water Proc. Eng.*, 2024, **67**, 106159.
76 X. Wei, *et al.*, Porous biochar supported Ag3PO4 photocatalyst for "two-in-one" synergistic adsorptive-photocatalytic removal of methylene blue under visible light irradiation, *J. Environ. Chem. Eng.*, 2021, **9**(6), 106753.
77 C. Zhang, *et al.*, Extended construction strategies of Ag3PO4-based heterojunction photocatalysts for robust environmental applications, *J. Environ. Chem. Eng.*, 2023, **11**(5), 110705.
78 S. Ghosh and M. Sahu, Biochar Supported Oxygen Rich TiO2-CuO Heterojunction Photocatalyst for the Degradation of Dimethyl Phthalate: Optimization, Degradation Kinetics and Mechanisms, *Int. J. Environ. Res.*, 2025, **19**(2), 58.
79 H. Wang, N. J. Quitoriano and G. P. Demopoulos, Compact microstructured Cu2ZnSnS4 thin films with enhanced optoelectronic properties via (NH4) 2S tunable hybrid colloidal ink coating and transformation, *Colloids Surf., A*, 2024, **702**, 135065.
80 X. Li, *et al.*, Preparation of Fe3O4/FexSy heterostructures via electrochemical deposition method and their enhanced electrochemical performance for lithium-sulfur batteries, *Chem. Eng. J.*, 2022, **446**, 137267.
81 J. Wu, *et al.*, Efficient removal of microplastics from aqueous solution by a novel magnetic biochar: performance, mechanism, and reusability, *Environ. Sci. Pollut. Res.*, 2023, **30**(10), 26914–26928.
82 N. A. Anuwa-Amarh, *et al.*, Carbon-based adsorbents for microplastic removal from wastewater, *Materials*, 2024, **17**(22), 5428.
83 B. Song, *et al.*, Removal of PET Microfibers from Simulated Wastewater Using Magnetic Nano-Ferric-Loaded Biochar: High Adsorption and Regeneration Performance, *Nanomaterials*, 2025, **15**(12), 905.
84 S. Cairns, *et al.*, Interactions between biochar and nano (micro) plastics in the remediation of aqueous media, *Int. J. Environ. Res.*, 2024, **18**(5), 87.
85 R. L. Ramos, *et al.*, Critical review of microplastic in membrane treatment plant: Removal efficiency, environmental risk assessment, membrane fouling, and MP release, *Chem. Eng. J.*, 2024, **480**, 148052.
86 I. Ali, *et al.*, Interaction of microplastics and nanoplastics with natural organic matter (NOM) and the impact of NOM on the sorption behavior of anthropogenic contaminants–A critical review, *J. Clean. Prod.*, 2022, **376**, 134314.
87 D. Angeles-Beltrán, *et al.*, Photocatalytic degradation of phenol using cadmium-TiO2/chitosan hybrid catalysts, *Mater. Res. Express*, 2025, 2053.
88 A. Alaghmandfard and K. Ghandi, A comprehensive review of graphitic carbon nitride (g-C3N4)–metal oxide-based nanocomposites: potential for photocatalysis and sensing, *Nanomaterials*, 2022, **12**(2), 294.
89 P. Chen, *et al.*, Efficient removal of ciprofloxacin from water by BiOX/GaMOF S-scheme heterojunction: A synergistic effect of adsorption and photocatalysis, *Chem. Eng. J.*, 2025, 159689.
90 B. Gupta and A. K. Gupta, Photocatalytic performance of 3D engineered chitosan hydrogels embedded with sulfur-doped C3N4/ZnO nanoparticles for Ciprofloxacin removal: Degradation and mechanistic pathways, *Int. J. Biol. Macromol.*, 2022, **198**, 87–100.
91 X. Hu, *et al.*, Mechanisms underlying the photocatalytic degradation pathway of ciprofloxacin with heterogeneous TiO2, *Chem. Eng. J.*, 2020, **380**, 122366.
92 M. Delnavaz, S. Amiri and S. Najari, Highly efficient photocatalytic degradation of ciprofloxacin under simulated sunlight using g-C3N4/CeO2/Fe3O4 heterogeneous composite, *Ecotoxicol. Environ. Saf.*, 2025, **295**, 118175.
93 Y. Dong, *et al.*, A comprehensive study on the co-removal of Cr (VI) and ciprofloxacin via microbial-photocatalytic coupling: Mechanistic insights and performance evaluation, *J. Environ. Manage.*, 2024, **352**, 120044.
94 Y. Wang, *et al.*, Coupled piezo-pyro-photocatalysis of oxygen vacancies and Bi quantum dots co-modified BaTiO3 for highly efficient removal of ciprofloxacin, *Sep. Purif. Technol.*, 2024, **337**, 126392.
95 M.-T. Pham, *et al.*, Rapid and scalable fabrication of TiO2@ g-C3N4 heterojunction for highly efficient photocatalytic no removal under visible light, *Aerosol Air Qual. Res.*, 2021, **21**(12), 210276.
96 M. Pourmadadi, N. Aghababaei and M. Abdouss, Photocatalytic activation of peroxydisulfate by UV-LED through rGO/g-C3N4/SiO2 nanocomposite for ciprofloxacin removal: Mineralization, toxicity, degradation pathways, and application for real matrix, *Chemosphere*, 2024, **359**, 142374.
97 P. U. Iyare, S. K. Ouki and T. Bond, Microplastics removal in wastewater treatment plants: a critical review, *Environ. Sci.:Water Res. Technol.*, 2020, **6**(10), 2664–2675.
98 X. Luo, *et al.*, A review of analytical methods and models used in atmospheric microplastic research, *Sci. Total Environ.*, 2022, **828**, 154487.
99 K. Jedynak and B. Charmas, Adsorption properties of biochars obtained by KOH activation, *Adsorption*, 2024, **30**(2), 167–183.
100 H. Jiang, *et al.*, Multi-phase CdS loaded on biochar for photocatalytic activation of peroxymonosulfate for thiamethoxam degradation: π-conjugation improves PMS adsorption, *Sep. Purif. Technol.*, 2023, **326**, 124842.
101 X. Ji, *et al.*, Construction of Fe and g-C3N4 codoped magnetic bamboo charcoal for enhanced catalytic degradation of tetracycline: Mechanism, degradation pathway, and ecological toxicity, *Environ. Res.*, 2025, **266**, 120576.
102 T. Łęcki, *et al.*, Z-Scheme BiVO4/g-C3N4 Photocatalyst—With or Without an Electron Mediator?, *Molecules*, 2024, **29**(21), 5092.

103 S. Moosavi, *et al.*, Methylene blue dye photocatalytic degradation over synthesised Fe3O4/AC/TiO2 nanocatalyst: degradation and reusability studies, *Nanomaterials*, 2020, **10**(12), 2360.
104 D. Kanakaraju, M. A. B. Abdullah and L. Y. Chin, TiO2/PKSAC functionalized with Fe3O4 for efficient concurrent removal of heavy metal ions from water, *Colloid Interface Sci. Commun.*, 2021, **40**, 100353.
105 J. Chen, *et al.*, Synthesis of g-C3N4 composite co-doped with CeO2 and sugar cane bagasse charcoal for the degradation of methylene blue under visible light, *Colloids Surf., A*, 2022, **641**, 128551.
106 G. Yu, *et al.*, BiOCl-based composites for photocatalytic degradation of antibiotics: a review of synthesis method, modification, factors affecting photodegradation and toxicity assessment, *J. Alloys Compd.*, 2024, **981**, 173733.
107 S. Wang, *et al.*, Surface and interface engineering of BiOCl nanomaterials and their photocatalytic applications, *Adv. Colloid Interface Sci.*, 2024, **324**, 103088.
108 A. Nasir, *et al.*, A review on the progress and future of TiO2/graphene photocatalysts, *Energies*, 2022, **15**(17), 6248.
109 B. Yang, *et al.*, Synergy effect between tetracycline and Cr (VI) on combined pollution systems driving biochar-templated Fe3O4@ SiO2/TiO2/g-C3N4 composites for enhanced removal of pollutants, *Biochar*, 2023, **5**(1), 1.
110 A. Varadi, *et al.*, Fe3O4-ZnO: V nanocomposites with modulable properties as magnetic recoverable photocatalysts, *Inorganics*, 2024, **12**(4), 119.
111 M. M. Mian and G. Liu, Recent progress in biochar-supported photocatalysts: synthesis, role of biochar, and applications, *RSC Adv.*, 2018, **8**(26), 14237–14248.
112 F. Wu, *et al.*, Enhanced photocatalytic degradation and adsorption of methylene blue via TiO2 nanocrystals supported on graphene-like bamboo charcoal, *Appl. Surf. Sci.*, 2015, **358**, 425–435.
113 C. J. Pestana, *et al.*, A continuous flow packed bed photocatalytic reactor for the destruction of 2-methylisoborneol and geosmin utilising pelletised TiO2, *Chem. Eng. J.*, 2014, **235**, 293–298.
114 H. Qin, *et al.*, Adsorption of Pb2+ and Cd2+ in agricultural water by potassium permanganate and nitric acid-modified coconut shell biochar, *Agronomy*, 2023, **13**(7), 1813.
115 A. K. Badawi and B. Ismail, Recent progress in BiOX materials for efficient air pollutant degradation, *BiOX-based Photocatalysts for Dual Applications*, 2026, 505–516.
116 K. Wang, *et al.*, Biochar addition in membrane bioreactor enables membrane fouling alleviation and nitrogen removal improvement for low C/N municipal wastewater treatment, *Membranes*, 2023, **13**(2), 194.
117 K. Paritosh and N. Kesharwani, Biochar mediated high-rate anaerobic bioreactors: A critical review on high-strength wastewater treatment and management, *J. Environ. Manage.*, 2024, **355**, 120348.
118 B. Wang, *et al.*, Experiment investigation and multiscale modeling of biomass oxidative fast pyrolysis in a fluidized bed reactor, *Chem. Eng. J.*, 2024, **501**, 157546.
119 M. M. Bello, A. A. A. Raman and M. Purushothaman, Applications of fluidized bed reactors in wastewater treatment–a review of the major design and operational parameters, *J. Clean. Prod.*, 2017, **141**, 1492–1514.
120 H. Li, *et al.*, Wide-pH-compatible MoSx co-catalyst layer on TiO2 nanowire arrays photoanode for simultaneous acceleration of charge carrier separation and catalytic reactions, *Chem. Eng. J.*, 2022, **450**, 137900.
121 M. Song and J. Y. Park, Removal of microplastics in a hybrid treatment process of ceramic microfiltration and photocatalyst-mounted PES spheres with air backwashing, *Membranes*, 2024, **14**(8), 169.
122 H. Ullah, *et al.*, Biodegradation of microplastic: the role of aspergillus species in sustainable plastic waste management, *Med. Res. Rev.*, 2025, **3**(1), 314–329.
123 P. Romphophak, *et al.*, Removal of microplastics and nanoplastics in water treatment processes: A systematic literature review, *J. Water Proc. Eng.*, 2024, **64**, 105669.
124 A. Kumar, *et al.*, Recent advances in mechanistic insights into microplastics mitigation strategies via emerging advanced oxidation processes: Legislation, challenges, and future direction, *Sci. Total Environ.*, 2024, **957**, 177150.
125 D. Van Thuan, *et al.*, Photodegradation of ciprofloxacin antibiotic in water by using ZnO-doped g-C3N4 photocatalyst, *Chemosphere*, 2022, **308**, 136408.
126 Q. Liu, *et al.*, Current status of microplastics and nanoplastics removal methods: Summary, comparison and prospect, *Sci. Total Environ.*, 2022, **851**, 157991.
127 A. Boudouma, *et al.*, Electrodeposition synthesis of Cu2ZnSnS4 (CZTS) thin films as a promising material for photovoltaic cells: fundamentals, methods, and future prospects-a comprehensive review, *Mater. Today Sustain.*, 2024, 101018.
128 I. Ali, *et al.*, Recent innovations in microplastics and nanoplastics removal by coagulation technique: Implementations, knowledge gaps and prospects, *Water Res.*, 2023, **245**, 120617.
129 K. V. Gunavathy, *et al.*, Enhancing the optoelectronic performance of CZTS thin films through cobalt doping via nebulizer-assisted spray pyrolysis technique, *Sens. Actuators, A*, 2024, **366**, 114941.
130 M. Padervand, *et al.*, Removal of microplastics from the environment. A review, *Environ. Chem. Lett.*, 2020, **18**(3), 807–828.